Title: Leveraging genetic diversity to identify small molecules that reverse mouse skeletal muscle insulin resistance

Authors: Stewart W.C. Masson, Søren Madsen, Kristen C. Cooke, Meg Potter, Alexis Diaz-Vegas, Luke Carroll, Senthil Thillainadesan, Harry B. Cutler, Ken Walder, Gregory J. Cooney, Grant Morahan, Jacqueline Stöckli and David E. James

Abstract

Systems genetics has begun to tackle the complexity of insulin resistance by capitalising on computational advances to study high-diversity populations. “Diversity Outbred in Australia (DOz)” is a population of genetically unique mice with profound metabolic heterogeneity. We leveraged this variance to explore skeletal muscle’s contribution to whole-body insulin action through metabolic phenotyping and skeletal muscle proteomics of 215 DOz mice. Linear modelling identified 553 proteins that associated with whole-body insulin sensitivity (Matsuda Index) including regulators of endocytosis and muscle proteostasis. To enrich for causality, we refined this network by focussing on negatively associated, genetically regulated proteins, resulting in a 76-protein fingerprint of insulin resistance. We sought to perturb this network and restore insulin action with small molecules by integrating the Broad Institute Connectivity Map platform and *in vitro* assays of insulin action using the Prestwick chemical library. These complimentary approaches identified the antibiotic thiostrepton as an insulin resistance reversal agent. Subsequent validation in *ex vivo* insulin resistant mouse muscle, and palmitate induced insulin resistant myotubes demonstrated potent insulin action restoration, potentially via up-regulation of glycolysis. This work demonstrates the value of a drug-centric framework to validate systems level analysis by identifying potential therapeutics for insulin resistance.

Introduction

Skeletal muscle is a key determinant of whole-body glycaemic control. Under optimal conditions, insulin secreted from the pancreas initiates a signalling program in muscle, and other tissues, culminating in translocation of the insulin-responsive glucose transporter (GLUT4) to the plasma membrane (1). Increased plasma membrane GLUT4 lowers circulating glucose by increasing cellular influx for either storage as glycogen, or subsequent metabolism via the glycolytic pathway. Insulin resistance is the progressive failure of these processes, and often precedes a number of metabolic disorders including type 2 diabetes (2). Advances in genomics and computational biology have begun to shed new light on molecular drivers of insulin resistance. A recent study in humans undertook a GWAS of 188,577 individuals unveiling 53 genetic loci associated with a surrogate insulin resistance signature (3). Such studies are important as they point toward genetic lesions in metabolic tissues like skeletal muscle and adipose tissue as playing a key causal role in the development of insulin resistance. This emphasises the importance of focusing on genetics and peripheral tissues for new therapeutic targets and strategies to overcome insulin resistance. Recent developments in systems biology provides unique opportunities for discovering ways of reversing and or preventing insulin resistance. This will have enormous clinical benefit since insulin resistance is a gateway to an expanding family of diseases.

Over the past decade, genetically diverse mouse panels have been used to study metabolic disease (4-7). This is a major step forward because these panels combine control of the environment and access to any biological tissue, with a vast phenotypic and range which can be leveraged towards understanding complex diseases. Three specific resources are the hybrid mouse diversity panel (HMDP), and the BXD (C57BL/6J x DBA) and Collaborative Cross (CC) mouse strains (7-11). These panels comprise large selections of inbred mice spanning vast phenotypic and genetic landscapes. Collaborative Cross mice were first generated by interbreeding five commonly used laboratory mouse

48 strains (C57BL/6J, A/J, 129S1/SvlmJ, NZO/HILtJ, NOD/ShiLtJ) and three wild-derived strains (WSB/EiJ,
49 CAST/EiJ, PWK/PhJ) in a 'funnel' design. The resulting CC strains were then outbred to generate
50 Diversity Outbred mice at Jackson Laboratories (12) which have increased phenotypic diversity and
51 resolution for genetic mapping. An independent Diversity Outbred colony was established in Western
52 Australia using CC mice from Geniad (13). This colony has since relocated to our group at The
53 University of Sydney, termed Diversity Outbred mice from Australia (Oz) or DOz.

54

55 The use of such rodent models for studying complex traits has given rise to the field of Systems
56 Genetics. System genetics uses global quantification of 'intermediate phenotypes' i.e., gene
57 transcripts, proteins, metabolites to provide mechanistic links between genetic variation and complex
58 traits/disease (14, 15). Unlike traditional genetic studies that identify single or multiple loci of interest,
59 systems genetics often identifies entire biological pathways or networks that are inherently more
60 difficult to empirically test. In an attempt to streamline interrogation of molecular pathways, several
61 large-scale perturbation screens/projects have been undertaken. One such example is the Broad
62 Institute's Connectivity Map that integrated mRNA expression levels from 1.5 million combinations of
63 different cell lines and perturbations (small molecule inhibitors, receptor ligands, genetic
64 manipulations) into a searchable database (16-19). These kinds of tools provide invaluable resources
65 for testing hypotheses generated from systems genetics experiments, and for broadly linking
66 molecular networks to phenotypic outcomes.

67

68 Here we have utilised DOz mice to interrogate insulin resistance. By combining metabolic phenotyping
69 and skeletal muscle proteomics we have identified an insulin resistance fingerprint of 76 proteins. We
70 then used Connectivity Map to identify small molecules that give rise to an overlapping transcriptional
71 signature across a number of cell lines, and therefore have the potential to affect insulin action.
72 Strikingly, one of these compounds, the antibiotic thiostrepton, was also identified by us in an

independent small molecule screen for effectors of insulin action in myotubes. Subsequent validation of thiostrepton uncovered profound beneficial effects on insulin resistance *in vitro* and *ex vivo,* potentially via modulation of mitochondrial function and glycolysis.

Results

DOz metabolic and proteomic variation

Diversity Outbred from Oz (DOz) mice were metabolically phenotyped by oral glucose tolerance test (GTT) and echoMRI to determine body composition (Fig 1A-C). We integrated glucose and insulin levels during the GTT into a surrogate measure of whole-body insulin sensitivity referred to as the Matsuda Index (20). Similar to HOMA-IR, the Matsuda Index uses blood glucose and insulin values to predict whole-body insulin sensitivity. However, an advantage of the Matsuda Index over HOMA-IR is that it includes values over a range of GTT time-points, this better incorporates the dynamics of glycaemic control. Furthermore, the Matsuda Index is better correlated to the euglycemic-hyperinsulinaemic clamp, the gold standard measurement for insulin sensitivity, in humans (20). Consistent with studies in other DO mouse populations (12, 21), we observed profound phenotypic diversity in DOz mice with 20-to-400-fold differences in insulin sensitivity, adiposity, and fasting insulin levels across all DOz animals (Fig 1C). Notably, the metabolic variation we observed in DOz mice is markedly greater than the variation typically observed in similar studies using inbred mouse strains (Fig 1D). Since skeletal muscle, and mitochondrial function are major contributor to whole body insulin sensitivity in mammals (4, 22, 23), we performed proteomic analysis on quadriceps muscles that were fractionated into mitochondrial and post-mitochondrial fractions (PMF, Fig 1A). We identified 2073 total proteins (444 mitochondrial and 1629 PMF) present in at least 50% of mice. Mitochondrial proteins were defined based on their presence in MitoCarta 3.0 (24) and consistent with previous work (25) were approximately two-fold enriched in the mitochondrial fraction relative to the PMF (Fig 1E).

As with glycaemic control, muscle proteomes exhibited profound variation, with approximately 200-fold differences in coefficient of variation (CV) across both fractions (Fig 1F). Interestingly, glyceraldehyde-3-phosphate dehydrogenase (GAPDH), the often-reported western blot loading control was the 11th most variable protein in our dataset. Amongst the other highly variable proteins were the histone subunit H4F16, the mitochondrial iron-sulfur cluster assembly regulator ISCU, and the metalloendopeptidase OMA1. Among proteins with low variability between mice was the mitochondrial respiratory complex II subunit SDHA, and the 14-3-3 zeta isoform, YWHAZ. To uncover how variation differed across biological processes, gene ontology (GO) enrichment analysis was performed on proteins ranked by CV. Among the low variance processes were the electron transport chain (mitochondrial fraction) and regulation of chromosome organisation (PMF), while lipid metabolic pathways were highly variable across both mitochondrial and post-mitochondrial fractions (Fig 1G). As a control experiment, we also performed enrichment analysis on proteins ranked by LFQ relative abundance. High CV pathways (enriched for high CV proteins) tended to be lower in relative abundance (enriched for low relative abundance proteins) (Supplementary Fig 1a, b). However, many high variability pathways, lipid metabolism for example, were not enriched in either direction based on relative abundance suggesting differences in relative abundance do not fully explain pathway variability differences.

Role of skeletal muscle in whole-body insulin sensitivity

To leverage genetic and metabolic diversity toward uncovering new regulators of insulin action, we constructed linear models comparing insulin sensitivity (Matsuda Index) against protein abundance. Our initial analysis identified 37 mitochondrial and 40 PMF proteins that significantly associated with the Matsuda Index. Many of these appeared to be involved with adiposity rather than insulin action including adiponectin (ADIPOQ), adipsin (CFD), and the mitochondrial β-oxidation proteins ETFA and ETFB (Supplementary Fig 1C, D). Because we were mainly interested in identifying muscle-specific

123 factors that regulate insulin sensitivity, we next constructed a model that included adiposity (the
124 percentage of body mass which is adipose tissue) as a covariate. Using this approach, we identified
125 120 mitochondrial (Fig. 2A-B) and 433 PMF proteins that significantly associated with whole-body
126 insulin sensitivity. Comparison of the results from each model (with and without adiposity as a
127 covariate), revealed consensus proteins that associated with insulin sensitivity independently of
128 model design (Supplementary Fig 1E). These included the glycolytic enzymes PFKFB1 and PKM, which
129 have previously been identified as regulating muscle insulin action (4). Using adiposity as a covariate
130 not only increased the number of proteins identified but also uncovered relationships between
131 Matsuda Index and the GLUT4 trafficking regulators RAB10 (26, 27), SNAP23 (28) and IQGAP1 (29)
132 which were not seen in the original model. Comparison of the mitochondrial and PMF proteomes
133 revealed a mitochondrial enrichment for proteins that positively associate with insulin sensitivity,
134 highlighting the broadly positive role mitochondria play in muscle's contribution to metabolic health
135 (Fig 2C).

136

137 To gain further insight into the biology of skeletal muscle glycaemic control, we annotated candidate
138 proteins with PhosphoSite Plus data to test whether any protein of interest had documented roles in
139 metabolic signalling (Fig 2D-F). We observed no relationship between insulin signalling substrates and
140 regulation of whole-body insulin sensitivity (Fig 2D). However, there was a trend ($p = 0.08$) for AMPK
141 substrates in the PMF to be positively associated with insulin sensitivity. Interestingly, the most
142 positively (Canopy2; CNYP2) and most negatively (Rho GDP dissociation inhibitor alpha; ARHGDIA)
143 associated proteins were both annotated as being insulin responsive (Fig. 2F). We also preformed GO
144 gene-set enrichment analysis (GSEA) on proteins ranked by Matsuda Index effect sizes (Fig 2G). In the
145 PMF, 'response to topologically incorrect protein: GO:0051788' was positively associated with insulin
146 sensitivity while the 'proteasome complex: GO:0005839' and 'clathrin-coated pit: GO:0005905' were
147 negatively associated. Together the unfolded protein response and proteasome are indicative of the

role of proteostasis in insulin sensitivity (30, 31). Conversely, clathrin-coated pits play an important role in the internalisation of the insulin sensitive glucose transporter GLUT4 from the cell surface, a process negatively regulated by insulin (32-34). Consistent with our observation that the majority of the mitochondrial proteome is positively associated with insulin sensitivity, GSEA did not produce any negative results but did uncover a positive relationship between the mitochondrial respiratory complex I and Matsuda Index.

Integration of genetic linkage analysis and linear modelling with Connectivity Map

Changes in protein levels may be either cause or consequence of changes in insulin sensitivity. In an attempt to select for proteins with a potentially causal relationship, we performed genetic mapping analysis of both the mitochondrial and PMF proteomes (Fig 3A). Across both proteomes we identified 624 protein quantitative trait loci (pQTL). These were distributed across the genome and were predominately cis acting (Figure 3A), indicating that a significant proportion of variation in these proteins can be explained by their local genetic architecture. Next, we filtered proteins that were negatively associated with Matsuda Index by cis-pQTL presence to generate a molecular fingerprint of insulin resistance (Fig 3B). We focussed on negatively associated proteins based on the assumption that inhibiting deleterious proteins is easier than promoting the activity of beneficial ones. Filtering based on cis-pQTL presence was based on the rationale that if genetic variation can explain protein abundance differences between mice, then we can be confident that phenotype (Matsuda Index) is not driving the observed differences and therefore the protein-to-phenotype associations are likely causal. Importantly, this assumption can only be made for cis-acting pQTLs. Our analysis yielded a list of 76 (69 PMF and 7 mitochondrial) proteins that encompassed a wide range of biological processes (Supplementary Table 1). Low mitochondrial representation in the fingerprint is the result of selecting negatively associating proteins, and as seen (Figure 2C) previously, the mitochondrial proteome is enriched for positive contributors to insulin resistance. Similar approaches to identify molecular

phenotypes of insulin resistance have previously been conducted using collated human transcriptomic datasets (35-45). Using a compiled list from Timmons et al (46), we searched for orthologues of proteins from our fingerprint that associate with human insulin resistance. We identified four such genes (Fig. 3B): MTPN (myotrophin), LGALS1 (galectin 1), PHKB (phosphorylase b kinase), and ADPRHL1 (ADP-ribosylhydrolase Like 1), which may warrant further investigation.

To assess the tissue specificity of our fingerprint we searched for the same proteins in metabolically important adipose and liver tissues. Despite detecting 94% and 82% of muscle fingerprint proteins across each tissue respectively, both adipose and liver were depleted for pQTL presence (Figure 3C) suggesting that regulation of our candidate protein abundance is somewhat specific to skeletal muscle. Finally, we queried our fingerprint for any biological pathways that could represent novel drivers of insulin resistance by performing KEGG pathway enrichment (Fig 3C). Both 'endocytosis: mmu04144' (clathrin light chain A, clathrin light chain C, epidermal growth factor receptor pathway substrate 15) and 'insulin signalling pathway; mmu04910' (phosphorylase kinase regulatory subunit beta) featured in the top 10 providing further supportive evidence for the biological relevance of our fingerprint in the context of insulin sensitivity.

Next, we utilized Connectivity Map (CMAP) to convert our fingerprint into a list of small molecules and ligands that promote or oppose our muscle insulin resistance fingerprint. To test our assumption that pQTL filtering would improve our fingerprint we also queried CMAP with a list of the top 150 most strongly negatively associated proteins independent of pQTL presence. Intriguingly, on average CMAP scores for compounds and ligands were significantly higher when captured using a pQTL-filtered fingerprint compared to the non-pQTL filtered group, supporting the utility of this method (Supplementary Figure 2A). Encouragingly, the two highest scoring compounds identified using our fingerprint were Broad Institute glycogen synthase kinase (GSK3) and epidermal growth factor receptor (EGFR) inhibitors. Both of these kinases have been independently identified as drug targets

that reverse insulin resistance (37, 47, 48). Many compounds listed in the Connectivity Map database are proprietary Broad Institute inhibitors which are only identified by their Broad ID and cannot be easily procured for follow-up experiments. Therefore, we excluded all Broad Institute compounds from further analysis. After this filtering, 856 small molecules and 91 ligands generated gene expression signatures matching our query. As whole-body insulin sensitivity decreased with increased fingerprint protein abundance, we focussed on molecules whose CMAP score suggested a reversal of our insulin resistance fingerprint (Fig 3D). Ranking these candidates based on CMAP score revealed a number of well-known potentiators of insulin sensitivity including the antioxidant resveratrol (49), the diabetes medication metformin (50) and the growth factor FGF21 (51). We also identified the antibiotic thiostrepton (52), a documented proteasome inhibitor, consistent with our enrichment analysis which identified the proteasome as negatively contributing to insulin sensitivity.

Cross-validation of thiostrepton by Prestwick library screen of GLUT4 translocation

To obtain independent validation of some of the candidates revealed from Connectivity Map we performed a screen for compounds that affect GLUT4 translocation to the cell surface in L6 myotubes expressing HA-tagged GLUT4 (GLUT4-HA-L6), a readout of insulin action that is defective in insulin resistance. For this we used our established high sensitivity, high-throughput 96-well plate format screen that is amenable to physiological models of insulin resistance (53, 54), combined with the Prestwick library of FDA-approved drugs. In total, 420 compounds were found across both platforms, and these consensus compounds captured a significant proportion of highly scoring CMap compounds (Supplementary Figure 2C, D).

We performed 3 separate screens (Fig 4A) to capture the different mechanisms by which compounds modulate glucose uptake: 1) insulin-independent activation of GLUT4 translocation to the plasma membrane (basal activators), 2) potentiation of submaximal insulin action (insulin sensitisers), and 3) rescue of palmitate-induced insulin resistance (insulin resistance reversers). We identified 22 basal

agonists (Fig 4B), 7 insulin sensitisers (Fig 4C) and 16 insulin resistance reversers (Fig 4D). Five compounds both stimulated GLUT4 translocation and reversed insulin resistance, 4 were both basal agonists and insulin sensitisers while none met all three criteria (Fig 4E). Overall, we found that compounds that were identified by CMAP score (Fig 3D) performed better as both basal activators and as insulin resistance reversers than those that did not (Supplementary Fig 2B).

To cross-reference our CMAP data with the Prestwick screen in an unbiased way, we constructed a scoring matrix to rank compounds found by both our CMAP query and in the Prestwick library. First, we z-scored the values for each category (basal agonists, insulin sensitisers, insulin resistance reversal, CMAP score). Next, we averaged the three *in vitro* assays z-scores and added it to the CMAP score. This overall score represents how each compound modulates GLUT4 translocation, and potentially reverses our insulin resistance fingerprint, relative to the rest of the compound library. Using this final value, we ranked each compound and displayed the top 20 in a heat map (Fig 5A). Based on this metric, thiostrepton was identified as the highest-ranking compound and was selected for subsequent validation by further GLUT4 translocation (Fig. 5B) and 2-deoxyglucose uptake (Fig. 5C) experiments in GLUT4-HA-L6 myotubes. We observed a consistent reversal of insulin resistance across both assays.

Next, we assessed the efficacy of thiostrepton to reverse insulin resistance in diet-induced obese mice. We decided to study it in isolated muscles as this circumvents potentially confounding microbiome effects due to thiostrepton's antibiotic activity and allows direct interrogation of muscle insulin action. We selected two strains of inbred mice, C57BL/6J and BXH9/TyJ, based on our previous observations that these strains are particularly amenable to developing muscle insulin resistance following high-fat, high-sugar (western diet; WD) diet feeding (4). Consistent with diet-induced perturbations in metabolic health, both C57BL/6J and BXH9 BXH9/TyJ mice fed a WD had increased body weight and adiposity, fasting hyperglycemia, fasting hyperinsulinemia, glucose intolerance and lower systemic

248 insulin sensitivity (Matsuda Index) relative to chow-fed controls (Supplementary Fig. 3A-E). WD
249 feeding also resulted in ~40% reduction in C57BL/6J soleus insulin stimulated 2-deoxyglucose uptake,
250 a 75% reduction in BXH9 extensor digitorum longus insulin-stimulated 2-deoxyglucose uptake and
251 65% reduction in BXH9 soleus insulin stimulated 2-deoxyglucose uptake. Strikingly, 1 h of thiostrepton
252 treatment prior to insulin addition was sufficient to reverse 80% of WD-induced insulin resistance in
253 C57Bl/6J EDL muscle and 50% in BXH9 EDL muscle but did not restore BXH9 soleus 2-deoxyglucose
254 uptake (Figure 5D).

255

256 *Thiostrepton does not affect insulin signalling*

257 Next, we attempted to identify the potential mechanisms by which thiostrepton relieved insulin
258 resistance. Canonically, insulin stimulated GLUT4 translocation is facilitated by a signalling cascade
259 comprising PI3K/Akt and dysfunction in this pathway has been implicated in insulin resistance (55),
260 although this is controversial (2). To assess insulin signalling we treated control and palmitate-treated
261 GLUT4-HA-L6 myotubes with either thiostrepton or vehicle for 1 h prior to insulin stimulation. Unlike
262 GLUT4 translocation or 2-deoxyglucose uptake, palmitate did not perturb proximal insulin signalling.
263 We detected no effect of palmitate treatment or thiostrepton on the phosphorylation of Akt-T308,
264 Akt-S473, or the Akt-substrates GSK3-S21/9 and PRAS40-T246 (Fig. 6A-E). These findings are
265 consistent with the view that insulin resistance occurs independently of canonical insulin signalling
266 (56, 57) and suggests that thiostrepton is acting independently of signalling to reverse insulin
267 resistance.

268

269 *Thiostrepton partially inhibits mitochondria and restores palmitate induced glycolysis suppression*

270 Many insulin sensitising agents act via mitochondrial inhibition or uncoupling (58-60) and thiostrepton
271 has been reported to inhibit mitochondrial translation (61) and respiration (62, 63). To test whether

thiostrepton's ability to restore optimal insulin action occurs via mitochondria, palmitate-treated and control GLUT4-HA-L6 myotubes were incubated with thiostrepton as above. Consistent with the mitochondrial dysfunction that has been reported during insulin resistance (23, 64), we observed substantial suppression of maximal mitochondrial respiration and mitochondrial reserve capacity following palmitate treatment (Fig. 7A). Furthermore, thiostrepton alone appeared to blunt maximal respiration, albeit to a lesser extent than palmitate. When combined, thiostrepton and palmitate did not produce an additive suppression, nor did thiostrepton reverse any of the palmitate-induced defects. This suggests that this suppression of maximal respiration does not contribute to insulin resistance in this model.

We also assessed glycolysis by way of extra-cellular acidification rate (ECAR). Like mitochondrial respiration, palmitate suppressed maximal glycolytic capacity, however unlike respiration this was potently reversed by co-treatment with thiostrepton (Fig. 7B). To test whether this increase in glycolytic flux could be explained by changes in cellular energy status due to mitochondrial inhibition, we investigated the energy sensor AMP-dependent kinase (AMPK). AMPK can promote glycolysis (65), GLUT4 translocation (66, 67), and glucose uptake in skeletal muscle independently of insulin. However, unlike the AMPK activator A-769662, we observed no effect of thiostrepton on the phosphorylation of AMPK or its substrate acetyl-CoA carboxylase in either control cells or cells treated overnight with palmitate (Fig. 7C-E). Although A-769662 potently increases AMPK substrate phosphorylation in muscle cells, AMPK phosphorylation itself is not observed, consistent with a previous study (68). These data suggest that if thiostrepton activates glycolysis via mitochondrial inhibition, it occurs independently of AMPK.

Discussion

By leveraging genetic and phenotypic diversity of DOz mice we have explored skeletal muscle's contribution to whole-body insulin action at the molecular level. Our approach was validated by the identification of various 'positive controls' at each level of analysis. Firstly, utilising adiposity as a covariate during linear modelling uncovered relationships between whole-body insulin sensitivity and muscle GLUT4 trafficking proteins; secondly, pathway enrichment revealed proteostasis (30, 69) and endocytosis (32, 70) as key contributors to whole-body insulin sensitivity; and thirdly, querying Connectivity Map with our fingerprint of insulin resistance returned metformin, GSK3 (37, 71) and EGFR (47) inhibitors as potential insulin resistance therapeutics (50). The identification of these proteins, pathways and drugs by our strategy gives us confidence in our approach and the novel players identified.

Systems-based approaches often identify networks as being drivers of disease. Empirical validation of these is difficult due to the complex interactions in biological systems. Here we took a drug-centric approach to validate our findings; this allowed targeting of entire pathways rather than singular nodes. We identified several compounds across both *in silico* and *in vitro* analyses which may restore muscle insulin action, indeed several of these have previously been investigated. Disulfiram, sold under the brand name Antabuse, is used as an alcohol-dependency medication. Two studies have described disulfiram's ability to reverse diet-induced hepatic insulin resistance and reduce adiposity (72, 73). Resveratrol, a component found in red wine, is a popular antioxidant and has been demonstrated to reverse insulin resistance via reduction of reactive oxygen species (49, 74, 75). Fibroblast growth factor 21 (FGF21) was also identified amongst the ligand dataset as reversing our insulin resistance fingerprint. FGF21 has previously been reported to promote insulin-stimulated glucose uptake in muscle fibres (76) and can modulate mitophagy and proteostasis in muscle (77). Antivirals, several classes of antibiotics, antipsychotics and cancer drugs were all identified by our analyses. Perhaps this diversity reflects the divergent and pleiotropic biology of insulin resistance.

Key to our approach is the insulin resistance muscle proteomic fingerprint. This was generated by filtering proteins that associated with whole-body insulin sensitivity and that possessed significant cis-pQTLs. The latter was particularly important as we postulated that this would select for proteins that were likely to be causal drivers of insulin resistance. We hypothesed that a protein whose expression is post-translationally regulated in response to insulin resistance would not show a genetic signal and therefore be excluded from our fingerprint. Filtering on this basis improved the overall Connectivity Map score, and ultimately identified thiostrepton. One reason for this could be the discordance between mRNA and protein (78, 79). Connectivity Map uses mRNA expression data whereas our fingerprint uses protein. By restricting our fingerprint to proteins with significant cis-pQTLs we may have inadvertently selected for genes whose mRNA expression closely matches their protein thereby increasing the overlap between fingerprint and perturbagen signatures. Moreover, our approach has the major advantage that it requires far fewer mice to obtain meaningful outcomes (222 mice in this study) compared to that required for genetic mapping of complex traits like Matsuda Index (80)., Furthermore, because we have used genetically diverse datasets (DOz mice and multiple cell lines in Connectivity Map) our findings are likely robust across diverse target backgrounds.

A major question is what biological functions are represented by our fingerprint? One of the top pathways identified was endocytosis. This pathway featured two components of the clathrin coat and the adaptor protein EPS15. This is very exciting as endocytosis has been suggested to play a major role in stress signalling (81), and in the context of insulin sensitivity this may involve internalisation of key proteins including the insulin receptor and glucose or amino acid transporters (32, 70). The concept that variation in this process is genetically determined, and this plays a major role in governing essential processes like insulin action, adds a new dimension to the role of this pathway. A second intriguing member of the fingerprint is phosphorylase kinase which, along with glycogen synthase

kinase, regulates the key glycogen storage enzymes glycogen phosphorylase and glycogen synthase (82-85). High levels of glycogen phosphorylase kinase may promote glycogen breakdown through activation of glycogen phosphorylase thereby altering GSK3 signalling, a process implicated in insulin resistance.

Neither AMPK nor Akt signalling account for the profound effect of thiostrepton on insulin action. This is exciting as it suggests both a novel mechanism of action and a novel insulin resistance defect. So far, the most enticing potential mechanism is restoration of glycolysis. Thiostrepton restores normal glycolytic function in palmitate treated cells and we have previously reported links between glycolysis and insulin action in skeletal muscle (4, 86). Mechanistically, thiostrepton could promote glycolysis via attenuation of mitochondrial oxidative phosphorylation, and this has previously been demonstrated in acute myeloid leukemia and malignant mesothelioma cell lines (62, 87). Our data supports this work and identifies a similar, albeit mild, effect on myotube respiration. Thiostrepton can also increase cellular exposure to mitochondrial reactive oxygen species (ROS) as it inhibits peroxiredoxin-3 (63, 87), a key antioxidant enzyme. Perhaps, as seen during the Warburg effect (88-90), increased mitochondrial ROS can act as a signal to promote glycolysis and relieve mitochondrial energetic demands. Aside from glycolysis, other pathways may be involved in enhancing insulin sensitivity. For example, the negatively associated protein ARHGDIA (Figure 2F) is a potent negative regulator of insulin sensitivity, and our fingerprint of insulin resistance contained its homologue ARHGDIB. Both ARHGDIA and ARHGDIB have been reported to inhibit the insulin-action regulator RAC1 (91-93), and thus may lower GLUT4 translocation and glucose uptake. Further investigations may uncover a role for thiostrepton in modulating the RAC1 signalling pathway via ARHGDIB.

Integration of physiological, proteomic, genomic, and pharmaceutical data has uncovered a potent reverser of insulin resistance. By integrating proteomic diversity with the underlying genetic architecture, we believe we were able to focus on potentially causal proteins, and the use of

371 Connectivity Map allowed us to combine these proteins into a single fingerprint to find potential
372 modulators of insulin resistance. Our findings also build on recent reports linking glycolysis to insulin
373 action and uncover a number of potential contributors to insulin action worthy of future study.

374

Methods

Mouse breeding and phenotyping

Male 'Diversity Outbred from Oz' (DOz) mice were bred and housed at the Charles Perkins Centre, University of Sydney, NSW, Australia. They were originally established at Geniad, Western Australia, Australia and then relocated to The University of Sydney. The DOz population comprises 46 breeding pairs and the breeding strategy avoids mating's between siblings or first cousins. Breeders are selected based on the genotype of the *R2d2* locus to limit the meiotic drive favouring the WSB allele on chromosome 2 (94). The DOz mice used in the current study were outbred for 27 to 33 generations and comprised a total of 250 male DOz mice that were studied as 5 separate cohorts. Genomic DNA was isolated from each mouse and subjected to SNP genotyping (95), followed by genotyping diagnostics and cleaning as described (96). Experiments were performed in accordance with NHMRC guidelines and under approval of The University of Sydney Animal Ethics Committee. To delineate genetic from cage-effects, mice were randomised into cages of 3-5 at weaning. All mice were maintained at 23°C on a 12-hour light/dark cycle (0600-1800) and given *ad libitum* access to a standard laboratory chow diet containing 16% calories from fat, 61% calories from carbohydrates, and 23 % calories from protein or a high-fat high-sugar diet (western diet; WD) containing 45% calories from fat, 36% calories from carbohydrate and 19% calories from protein (3.5%g cellulose, 4.5%g bran, 13%g cornstarch, 21%g sucrose, 16.5%g casein, 3.4%g gelatine, 2.6%g safflower oil, 18.6%g lard, 1.2%g AIN-93 vitamin mix (MP Biomedicals), 4.95%g AIN-93 mineral mix (MP Biomedicals), 0.36%g choline and 0.3%g L-cysteine). Fat and lean mass measures were acquired via EchoMRI-900 (EchoMRI Corporation Pte Ltd, Singapore) at 14 weeks of age. Glucose tolerance was determined by oral glucose tolerance test (GTT) at 14-weeks of age by fasting mice for 6-hours (0700-1300 hrs) before oral gavage of 20% glucose solution in water at 2 mg/kg lean mass. Blood glucose concentrations was measured directly by handheld glucometer (Accu-Chek, Roche Diabetes Care, NSW, Australia) from tail blood 0, 15, 30, 45, 60, 90 minutes after oral gavage of glucose. Blood insulin levels at the 0- and 15-minute time points were measured by mouse insulin ELISA Crystal Chem USA (Elk Grove Village, IL, USA) according to

manufacturer instructions. Blood glucose and insulin levels were integrated into a surrogate measure of whole-body insulin sensitivity using the Matsuda Index:

$$Matsuda\ Index = \frac{10{,}000}{\sqrt{(Glucose_0 \times Insulin_0) \times (Glucose_{\mathrm{GTT}\ mean} \times Insulin_{GTT\ mean})}}$$

Muscle proteomic sample prep

Whole quadriceps muscle samples were prepared as previously described with modification (97, 98). First, tissue was snap frozen with liquid nitrogen and pulverized before resuspension in 100 µL of trypsin buffer (phosphate buffered saline; PBS containing 10 mM EDTA and 0.01 ug/uL mass-spectrometry grade trypsin). Samples were incubated for 30 minutes at 37 °C before being pelleted by centrifugation (10,000 g, 5 minutes at 4 °C). Samples were then resuspended in 1.4 mL mitochondrial isolation buffer (70 mM sucrose, 220 mM Mannitol, 1 mM EGTA, 2 mM HEPES. pH at 7.4) and homogenised on ice in a glass Dounce homogeniser. Samples were then twice pelleted by centrifugation, first at 1000 g x 10 min to remove insoluble debris and second at 10,000 g x 10 min to extract the crude mitochondrial fraction, both centrifugation steps were performed at 4 °C and the supernatant of the second step was collected as the post-mitochondrial fraction (PMF). The mitochondrial pellet was re-solubilised in 1 mL of isolation buffer by repeated pipetting on ice prior to centrifugation (10.000 g x 10 min at 4*C) and resuspension in 50 µL of isolation buffer. Protein concentration of both mitochondrial and PMF was determined by BCA assay, 10 µg of protein was then prepared as previously described (4). Reduction/alkylation (10mM TCEP, 40mM CAA) buffer was added to each sample before incubation for 20 minutes at 60 °C. Once cooled to room temperature, 0.4 mg trypsin and 0.4 mg LysC was added to each sample and incubated overnight (18h) at 37C with gentle agitation. 30µL water and 50 µL 1% TFA in ethyl acetate was added to stop digestion and dissolve any precipitated SDC. Samples were prepared for mass spectrometry analysis by StageTip

clean up using SDB-RPS solid phase extraction material (99). Briefly, 2 layers of SDB-RPS material was packed into 200 µL tips and washed by centrifugation at 1,000 x g for 2 minutes with 50 µL acetonitrile followed by 0.2% TFA in 30% methanol and then 0.2% TFA in water. 50 µL of samples were loaded to StageTips by centrifugation at 1,000 g for 3 minutes. Stage tips were washed with subsequent spins at 1,000 g for 3 minutes with 50 µL 1% TFA in ethyl acetate, then 1% TFA in isopropanol, and 0.2% TFA in 5% ACN. Samples were eluted by addition of 60µL 60% ACN with 5% NH_4OH_4. Samples were dried by vacuum centrifugation and reconstituted in 30 µL 0.1% TFA in 2% ACN.

Mass spectrometry analysis

Proteomic sample analysis was conducted using a Dionex UltiMate 3000 RSLCnano LC coupled to a Exploris Orbitrap mass spectrometer. 2 µL of sample was injected on to an in-house packed 150 µm x 15 cm column (1.9 mm particle size, ReproSilPurC18-AQ) and separated using a gradient elution and with column temperature of 60 °C, with Buffer A consisting of 0.1% formic acid in water and Buffer B consisting of 0.1% formic acid in 80% ACN. Samples were loaded to the column at a flow rate 3 µL min^{-1} at 3% B for 3 minutes, before dropping to 1.2 µL min^{-1} over 1 minute for the gradient elution. The gradient was increased to 32% B over 50 min, then to 60% B over 0.5 min and 98% B over 0.5 min and held for 1.5 min, before returning to a flow rate of 3 µL min^{-1} at 3% B. Eluting peptides were ionized by electrospray with a spray voltage of 2.3kV and a transfer capillary temperature of 300 °C. Mass spectra were collected using a DIA method with varying isolation width windows (widths of *m/z* 22-589) between 350 - 1650 according to Table S1. MS1 spectra were collected between *m/z* 350-1650 at a resolution of 60,000 and an AGC target of 4e5 with a 50 ms maximum injection time. Ions were fragmented with stepped HCD collision energy at 27.5% and MS2 spectra collected between m/z 300-2000 at resolution of 30,000, with an AGC target of 3e5 and the maximum injection time of 54 ms.

Proteomics raw data files were searched using DIA-NN using a library free FASTA search against the reviewed UniProt mouse proteome (downloaded May 2020) with deep learning enabled (99, 100). The protease was set to Trypsin/P with 1 missed cleavage, N-term M excision, carbamidomethylation and M oxidation options on. Peptide length was set to 7-30, precursor range 350-1650, and fragment range 300-2000, and FDR set to 1%. Both the PMF and mitochondrial fractions were filtered for mitochondrial proteins using based on MitoCarta 3.0 and presence in 50% in mice. Across both fractions we quantified 2073 proteins (1629 proteins in the PMF and 444 in the mitochondrial fraction). Proteomic intensities were log2 transformed and median normalised prior to analysis to achieve normal distributions and account for technical variation in total protein. The mass spectrometry proteomics data have been deposited to the ProteomeXchange Consortium via the PRIDE (101) partner repository with the dataset identifier PXD042277.

Data analysis

All data analysis and visualisation was performed in either the R programming environment (102) or GraphPad Prism (GraphPad Software, San Diego, California USA). For protein-trait analysis the Matsuda Index was calculated using glucose tolerance data before being log2 transformed. Linear models were generated using the *lm()* function in R where Matsuda Index = α + proteinX + covariate + ε (α = intercept and ε = error) using a gaussian distribution. To correct for multiple testing, p-values were adjusted using the q-value method in the R package *qvalue* (103). Chi-square tests for distribution differences within the data and two/one-way ANOVA tests for group differences were performed in GraphPad Prism.

Gene-set enrichment

Gene-set enrichment analysis for each mitochondrial and post-mitochondrial fraction was conducted using Matsuda Index effect sizes for each protein and performed in R using the *gseGO()* function within the clusterprofiler package (104). Over-representation analysis of protein-protein interaction clusters and KEGG pathway analysis of insulin resistance fingerprint proteins were performed in WebGestalt (105). All enrichment tests were performed using all quantified proteins within a given fraction as a background gene-set. P-value correction was performed using false-discovery rate correction.

Genetic mapping analysis

Genetic mapping analysis was performed in R using the QTL2 package (106). The GIGA-MUGA single nucleotide polymorphism array was used as genomic inputs for mapping (95). pQTL analysis was performed by linear mixed modelling on z-scored protein abundance data with probabilistic estimation of expression residuals (PEER) factor adjustment, a covariate, and a kinship matrix to account for genetic relatedness amongst the DOz animals. PEER factor adjustment was performed using the top 10 calculated PEER factors, as described (107). Significance thresholds were established by performing 1000 permutations and set at $P < 0.1$ for cis-acting pQTL and $P < 0.05$ for trans acting pQTL. The cis-pQTL window was set as ± 2 Mbp.

Connectivity Map and scoring matrix

Insulin resistance 'fingerprint' proteins were queried in Connectivity Map using the CLUE software platform (16, 19). The list of 76 'fingerprint proteins' were queried against the L1000 gene expression dataset in the "Query" function of CLUE and results for small molecules (trt_cp) and ligands (trt_lig) were extracted using the CLUE "Morpheus" platform. Raw connectivity score values were used to rank perturbagens. Connectivity scores were averaged across all cell lines in the L1000 dataset. The Broad Institute small molecule inhibitors denoted by the prefix were removed from our resulting dataset as

they are not commercially available. Connectivity Map scores were combined with the results from our GLUT4 translocation screen to rank consensus compounds. This was done by first z-scoring each value (% GLUT4 at the plasma membrane for each assay and raw connectivity score). This produced a value which indicates how well each compound performs in a given test relative to the rest of the dataset. Then the average of all three GLUT4 assays (basal agonism, insulin sensitisation, and insulin resistance reversal) was added to the z-scored Connectivity Score to produce an overall score for each compound. Z-score adjustment for each assay and CMAP score was performed as follows:

$$Zscore = \frac{x - mean}{SD}$$

Where:

- Zscore = adjusted value for a given compound
- x = observed score for given compound
- mean = average score across all compounds
- SD = standard deviation of all compounds

Overall score for each compound was calculated as follows:

$$\frac{\text{z-scored}\ (bas) + \text{z-scored}\ (ins.sens) + \text{z-scored}\ (ins.res.rev)}{3} + \text{z-scored}\ (CMAP)$$

$$= Overall\ score$$

Cell culture

GLUT4-HA-L6 myoblasts (108) were grown in α-MEM supplemented with 10% fetal bovine serum. Differentiation was induced by changing media to α-MEM supplemented with 2% horse serum for 5 days.

GLUT4 translocation assays

GLUT4 exocytosis was determined as previously reported (53). Briefly, GLUT4-HA-L6 myotubes were serum starved overnight in α-MEM containing 0.2% BSA before being washed 3x with Krebs Ringer phosphate buffer supplemented with 0.2% BSA. Cells were stimulated with either 1 nM or 100 nM insulin for 20 minutes before being washed with ice-cold PBS and placed on ice. Cells were then fixed for 30 minutes in 3% paraformaldehyde, washed with phosphate buffered saline. Remaining paraformaldehyde was quenched with 50 mM glycine. Cells were then blocked for 20 minutes in either 5% normal swine serum (NSS) or 5% NSS with 0.1% saponin (for measurement of total GLUT4 levels). After blocking cells were washed and incubated with anti-HA antibody (Convance, 1:200 in 5% NSS) for 45 minutes before incubation with secondary antibody for 20 minutes. Total and plasma membrane GLUT4-HA was determined by fluorescence plate reader at 485/520 nm. GLUT4 translocation was calculated as % of total GLUT4 at the plasma membrane. For palmitate induced insulin resistance assays myotubes were incubated in αMEM overnight supplemented with either 125 µM palmitic acid conjugated to BSA or equivalent BSA as a vehicle control before performing assay as above. For assessment of the Prestwick library of compounds, each compound was dissolved in DMSO and added for 1 hour at a final concentration of 10 µM (0.2% DMSO) prior to experimentation. Biological significance for each assay was defined as 50% of control. For basal agonists this was > 50% of 100 nM insulin, for insulin sensitisers this was > 50% of the difference between 1 and 100 nM insulin, and for insulin resistance reversers this was > 50% of the difference between 100 nM insulin and 100 nM insulin + palmitate.

2-deoxyglucose uptake

2-deoxyglucose uptake into GLUT4-HA-L6 cells was performed as previously described with modifications (108, 109). Cells were incubated overnight in either αMEM overnight supplemented with either BSA-coupled 125 µM palmitic acid or BSA vehicle control before being washed 3x with HEPES buffed saline (HBS). Cells were then incubated in HBS supplemented with 10 µM unlabelled 2-

deoxyglucose and 0.5 µCi/ml [^{3}H]-2-deoxyglucose at 37°C for 5 minutes. Cells were then washed 5x with ice-cold PBS and lysed in 1M NaOH. For non-specific background uptake, 1 well per condition was pre-treated with cytochalasin B. Counts were determined by Perkin Elmer Quantulus GCT Liquid Scintillation Counter (Perkin Elmer, Waltham, MA, USA). Glucose uptake was expressed relatively to protein concentration as determined by bicinchoninic acid (BCA) assay after subtraction of non-specific uptake.

Ex vivo glucose uptake

Ex vivo glucose uptake was performed as previously described (4). Mice were euthanized by cervical dislocation prior to rapid dissection of soleus (C57Bl/6J and BXH9/TyJ) and extensor digitorum longus (EDL) muscle (BXH9/TyJ only). Muscle selection was based on our prior observations that only soleus muscles in C57Bl/6J mice develop diet-induced insulin resistance. Both the soleus and EDL muscles were mounted and then incubated for 1 h in Krebs Henseleit buffer (KHB; 5.5 mM glucose, 2 mM pyruvate and 0.1% BSA) that had been gassed with carbogen (95% O2/5% CO2) supplemented with either 10 µM thiostrepton or a DMSO vehicle control. Glucose uptake was assessed by then switching the muscle into KHB supplemented with 0.375 mCi/ml [3H]-2-dexoyglucose (2-DG), 0.05 mCi/ml [14C]-Mannitol, 100 nM insulin and either thiostrepton (10 µM) or DMSO vehicle control for 20 minutes at 30 °C followed by washing in ice-cold PBS and then snap frozen in liquid nitrogen. Samples were lysed in 250 mM NaOH at 70 °C. Tracer in the muscle tissue lysates was quantified by liquid scintillation counting and [3H]-2-DG was corrected for extracellular [14C]-mannitol then normalized to wet weight of the tissue.

Immunoblotting

Glut4-HA-L6 myotubes were incubated overnight in 125 µM palmitate or BSA control prior to treatment with drugs/insulin as indicated. Cells were then washed in ice-cold PBS and lysed by scraping directly into 55 °C Laemmli sample buffer with 10 % (tris 2-carboxyethyl phosphine; TCEP). Samples were then sonicated for 24 s (3s on/3s off) and heated at 65 °C for 5 minutes. SDS-PAGE was performed. Samples were resolved by SDS-PAGE as previously described (4), transferred onto PVDF membranes and blocked in TBS-T (0.1% Tween in Tris-buffered saline) containing 5% skim milk for 1 hour. Membranes were then washed 3 x 10 minutes in TBS-T and incubated overnight in primary antibodies against phosphorylated Akt T308 (Cell Signaling Technologies #2965; diluted 1:1000), phosphorylated Akt S473 (Cell Signaling Technologies #9271; diluted 1:1000), pan-Akt (Cell Signaling Technologies #9272; diluted 1:1000), phosphorylated GSK-3α/β S21/9 (Cell Signaling Technologies #9327; diluted 1:1000), GSK3α/β (Cell Signaling Technologies #5676; diluted 1:1000), phosphorylated PRAS40 T246 (Cell Signaling Technologies #13175; diluted 1:1000), PRAS40 (Cell Signaling Technologies #2691; diluted 1:1000), phosphorylated AMPK (Cell Signaling Technologies, #2531; diluated 1:1000), α-tubulin (Cell Signalling Technologies #2125; diluted 1:1000), 14-3-3 (Santa Cruz #sc-1657; diluted 1:5000) . The following day membranes were washed 3 x 10 minutes in TBS-T and incubated for 1 hour in species-appropriate fluorescent or HRP secondary antibodies. Imaging and densitometry were performed using LI-COR Image Studio or a Bio-Rad ChemiDoc Imaging System (Bio-Rad, Hercules, CA, USA) and Image J (110). Phosphorylated proteins were normalised against their relevant controls and data was normalised based on average band intensity.

Mitochondrial stress test

Cellular respirometry (oxygen consumption rate, OCR) was performed using Seahorse XFp miniplates and a Seahorse XF HS Mini Analyzer (Seahorse Bioscience, Copenhagen, Denmark) as previously described (111). GLUT4-HA-L6 myotubes were incubated overnight in either palmitate or BSA control αMEM before treatment with either thiostrepton (10 µM) or DMSO vehicle control. Cells were washed

591 twice with KRBH and incubated in KRBH supplemented with 2.8 mM glucose, thiostrepton or vehicle
592 control without BSA (150 µl/well) at 37°C for 1h in non-CO2 incubator. Cells were then assayed in XFp
593 Analyzer. The OCR was measured after a 12-min equilibration period followed by 3/0/3 min of
594 mix/wait/read cycles. Following stabilization of baseline rates, compounds were injected sequentially
595 to reach a final concentration of: 20 mM glucose, oligomycin (5µg/ml), FCCP (1 µM) and
596 rotenone/antimycin A (5 µM) to assess glucose-dependent respiration (calculated by baseline –
597 glucose OCR), ATP-linked respiration (determined by glucose – oligomycin OCR), maximal respiration
598 (calculated by FCCP – AntA/Rot OCR) and non-mitochondrial respiration respectively (equal to
599 AntA/Rot OCR). Data were normalised against protein concentration and presented as baseline
600 adjusted.

601

602 Acknowledgements

603 This work is dedicated to our wonderful colleague and friend Senthil Thillainadesan (1988-2023). We'd
604 like to thank the Sydney Mass Spectrometry facility in the Charles Perkins Centre at the University of
605 Sydney for mass spectrometry support. We'd also like to thank Large Animal Services in the Charles
606 Perkins Centre at The University of Sydney for mouse housing support, and Cordula Hohnen-Behrens,
607 Nicky Konstantopoulos and Briana Spolding for *in vitro* GLUT4 translocation assay assistance.

608

609 1. Bryant NJ, Govers R, James DE. Regulated transport of the glucose transporter GLUT4. Nat Rev
610 Mol Cell Biol. 2002;3(4):267-77.
611 2. James DE, Stockli J, Birnbaum MJ. The aetiology and molecular landscape of insulin resistance.
612 Nat Rev Mol Cell Biol. 2021;22(11):751-71.
613 3. Lotta LA, Gulati P, Day FR, Payne F, Ongen H, van de Bunt M, et al. Integrative genomic analysis
614 implicates limited peripheral adipose storage capacity in the pathogenesis of human insulin resistance.
615 Nat Genet. 2017;49(1):17-26.
616 4. Nelson ME, Madsen S, Cooke KC, Fritzen AM, Thorius IH, Masson SW, et al. Systems-level
617 analysis of insulin action in mouse strains provides insight into tissue-and pathway-specific
618 interactions that drive insulin resistance. Cell Metab. 2022.
619 5. Parks BW, Sallam T, Mehrabian M, Psychogios N, Hui ST, Norheim F, et al. Genetic architecture
620 of insulin resistance in the mouse. Cell Metab. 2015;21(2):334-47.

6. Williams EG, Wu Y, Jha P, Dubuis S, Blattmann P, Argmann CA, et al. Systems proteomics of liver mitochondria function. Science. 2016;352(6291):aad0189.
7. Yang CH, Mangiafico SP, Waibel M, Loudovaris T, Loh K, Thomas HE, et al. E2f8 and Dlg2 genes have independent effects on impaired insulin secretion associated with hyperglycaemia. Diabetologia. 2020;63(7):1333-48.
8. Ghazalpour A, Rau CD, Farber CR, Bennett BJ, Orozco LD, van Nas A, et al. Hybrid mouse diversity panel: a panel of inbred mouse strains suitable for analysis of complex genetic traits. Mamm Genome. 2012;23(9-10):680-92.
9. Ashbrook DG, Arends D, Prins P, Mulligan MK, Roy S, Williams EG, et al. A platform for experimental precision medicine: The extended BXD mouse family. Cell Syst. 2021;12(3):235-47.e9.
10. Peirce JL, Lu L, Gu J, Silver LM, Williams RW. A new set of BXD recombinant inbred lines from advanced intercross populations in mice. BMC Genet. 2004;5:7.
11. Consortium CC. The genome architecture of the Collaborative Cross mouse genetic reference population. Genetics. 2012;190(2):389-401.
12. Svenson KL, Gatti DM, Valdar W, Welsh CE, Cheng R, Chesler EJ, et al. High-resolution genetic mapping using the Mouse Diversity outbred population. Genetics. 2012;190(2):437-47.
13. Ferguson B, Handoko HY, Mukhopadhyay P, Chitsazan A, Balmer L, Morahan G, et al. Different genetic mechanisms mediate spontaneous versus UVR-induced malignant melanoma. Elife. 2019;8.
14. Baliga NS, Björkegren JLM, Boeke JD, Boutros M, Crawford NPS, Dudley AM, et al. The State of Systems Genetics in 2017. Cell Systems. 2017;4(1):7-15.
15. Seldin M, Yang X, Lusis AJ. Systems genetics applications in metabolism research. Nature metabolism. 2019;1(11):1038-50.
16. Subramanian A, Narayan R, Corsello SM, Peck DD, Natoli TE, Lu X, et al. A Next Generation Connectivity Map: L1000 Platform and the First 1,000,000 Profiles. Cell. 2017;171(6):1437-52.e17.
17. Uva P, Bosco MC, Eva A, Conte M, Garaventa A, Amoroso L, et al. Connectivity Map Analysis Indicates PI3K/Akt/mTOR Inhibitors as Potential Anti-Hypoxia Drugs in Neuroblastoma. Cancers (Basel). 2021;13(11).
18. Lamb J, Crawford ED, Peck D, Modell JW, Blat IC, Wrobel MJ, et al. The Connectivity Map: using gene-expression signatures to connect small molecules, genes, and disease. Science. 2006;313(5795):1929-35.
19. Lamb J. The Connectivity Map: a new tool for biomedical research. Nat Rev Cancer. 2007;7(1):54-60.
20. Matsuda M, DeFronzo RA. Insulin sensitivity indices obtained from oral glucose tolerance testing: comparison with the euglycemic insulin clamp. Diabetes Care. 1999;22(9):1462-70.
21. Churchill GA, Gatti DM, Munger SC, Svenson KL. The Diversity Outbred mouse population. Mamm Genome. 2012;23(9-10):713-8.
22. DeFronzo RA. Lilly lecture 1987. The triumvirate: beta-cell, muscle, liver. A collusion responsible for NIDDM. Diabetes. 1988;37(6):667-87.
23. Anderson EJ, Lustig ME, Boyle KE, Woodlief TL, Kane DA, Lin C-T, et al. Mitochondrial H2O2 emission and cellular redox state link excess fat intake to insulin resistance in both rodents and humans. The Journal of Clinical Investigation. 2009;119(3):573-81.
24. Rath S, Sharma R, Gupta R, Ast T, Chan C, Durham TJ, et al. MitoCarta3.0: an updated mitochondrial proteome now with sub-organelle localization and pathway annotations. Nucleic Acids Res. 2021;49(D1):D1541-d7.
25. Williams EG, Wu Y, Wolski W, Kim JY, Lan J, Hasan M, et al. Quantifying and Localizing the Mitochondrial Proteome Across Five Tissues in A Mouse Population. Mol Cell Proteomics. 2018;17(9):1766-77.
26. Su Z, Deshpande V, James DE, Stockli J. Tankyrase modulates insulin sensitivity in skeletal muscle cells by regulating the stability of GLUT4 vesicle proteins. J Biol Chem. 2018;293(22):8578-87.
27. Chen Y, Lippincott-Schwartz J. Rab10 delivers GLUT4 storage vesicles to the plasma membrane. Commun Integr Biol. 2013;6(3):e23779.

672 28. Kawanishi M, Tamori Y, Okazawa H, Araki S, Shinoda H, Kasuga M. Role of SNAP23 in insulin-
673 induced translocation of GLUT4 in 3T3-L1 adipocytes. Mediation of complex formation between
674 syntaxin4 and VAMP2. J Biol Chem. 2000;275(11):8240-7.
675 29. Chawla B, Hedman AC, Sayedyahossein S, Erdemir HH, Li Z, Sacks DB. Absence of IQGAP1
676 Protein Leads to Insulin Resistance. J Biol Chem. 2017;292(8):3273-89.
677 30. Díaz-Ruiz A, Guzmán-Ruiz R, Moreno NR, García-Rios A, Delgado-Casado N, Membrives A, et
678 al. Proteasome Dysfunction Associated to Oxidative Stress and Proteotoxicity in Adipocytes
679 Compromises Insulin Sensitivity in Human Obesity. Antioxidants & redox signaling. 2015;23(7):597-
680 612.
681 31. Minard AY, Wong MK, Chaudhuri R, Tan SX, Humphrey SJ, Parker BL, et al. Hyperactivation of
682 the Insulin Signaling Pathway Improves Intracellular Proteostasis by Coordinately Up-regulating the
683 Proteostatic Machinery in Adipocytes. J Biol Chem. 2016;291(49):25629-40.
684 32. Antonescu CN, Díaz M, Femia G, Planas JV, Klip A. Clathrin-dependent and independent
685 endocytosis of glucose transporter 4 (GLUT4) in myoblasts: regulation by mitochondrial uncoupling.
686 Traffic. 2008;9(7):1173-90.
687 33. Robinson LJ, Pang S, Harris DS, Heuser J, James DE. Translocation of the glucose transporter
688 (GLUT4) to the cell surface in permeabilized 3T3-L1 adipocytes: effects of ATP insulin, and GTP gamma
689 S and localization of GLUT4 to clathrin lattices. J Cell Biol. 1992;117(6):1181-96.
690 34. Fazakerley DJ, Holman GD, Marley A, James DE, Stöckli J, Coster AC. Kinetic evidence for
691 unique regulation of GLUT4 trafficking by insulin and AMP-activated protein kinase activators in L6
692 myotubes. J Biol Chem. 2010;285(3):1653-60.
693 35. Sears DD, Hsiao G, Hsiao A, Yu JG, Courtney CH, Ofrecio JM, et al. Mechanisms of human
694 insulin resistance and thiazolidinedione-mediated insulin sensitization. Proceedings of the National
695 Academy of Sciences of the United States of America. 2009;106(44):18745-50.
696 36. Gallagher IJ, Scheele C, Keller P, Nielsen AR, Remenyi J, Fischer CP, et al. Integration of
697 microRNA changes in vivo identifies novel molecular features of muscle insulin resistance in type 2
698 diabetes. Genome Med. 2010;2(2):9.
699 37. Leng S, Zhang W, Zheng Y, Liberman Z, Rhodes CJ, Eldar-Finkelman H, et al. Glycogen synthase
700 kinase 3 beta mediates high glucose-induced ubiquitination and proteasome degradation of insulin
701 receptor substrate 1. J Endocrinol. 2010;206(2):171-81.
702 38. Josse AR, Atkinson SA, Tarnopolsky MA, Phillips SM. Increased consumption of dairy foods and
703 protein during diet- and exercise-induced weight loss promotes fat mass loss and lean mass gain in
704 overweight and obese premenopausal women. J Nutr. 2011;141(9):1626-34.
705 39. Phillips BE, Williams JP, Gustafsson T, Bouchard C, Rankinen T, Knudsen S, et al. Molecular
706 networks of human muscle adaptation to exercise and age. PLoS Genet. 2013;9(3):e1003389.
707 40. Sood S, Gallagher IJ, Lunnon K, Rullman E, Keohane A, Crossland H, et al. A novel multi-tissue
708 RNA diagnostic of healthy ageing relates to cognitive health status. Genome Biol. 2015;16(1):185.
709 41. Barberio MD, Huffman KM, Giri M, Hoffman EP, Kraus WE, Hubal MJ. Pyruvate Dehydrogenase
710 Phosphatase Regulatory Gene Expression Correlates with Exercise Training Insulin Sensitivity Changes.
711 Med Sci Sports Exerc. 2016;48(12):2387-97.
712 42. Espah Borujeni A, Mishler DM, Wang J, Huso W, Salis HM. Automated physics-based design of
713 synthetic riboswitches from diverse RNA aptamers. Nucleic Acids Res. 2016;44(1):1-13.
714 43. Hangelbroek RW, Fazelzadeh P, Tieland M, Boekschoten MV, Hooiveld GJ, van Duynhoven JP,
715 et al. Expression of protocadherin gamma in skeletal muscle tissue is associated with age and muscle
716 weakness. Journal of cachexia, sarcopenia and muscle. 2016;7(5):604-14.
717 44. Nakhuda A, Josse AR, Gburcik V, Crossland H, Raymond F, Metairon S, et al. Biomarkers of
718 browning of white adipose tissue and their regulation during exercise- and diet-induced weight loss.
719 Am J Clin Nutr. 2016;104(3):557-65.
720 45. Phillips BE, Kelly BM, Lilja M, Ponce-González JG, Brogan RJ, Morris DL, et al. A Practical and
721 Time-Efficient High-Intensity Interval Training Program Modifies Cardio-Metabolic Risk Factors in
722 Adults with Risk Factors for Type II Diabetes. Front Endocrinol (Lausanne). 2017;8:229.

46. Timmons JA, Atherton PJ, Larsson O, Sood S, Blokhin IO, Brogan RJ, et al. A coding and non-coding transcriptomic perspective on the genomics of human metabolic disease. Nucleic Acids Research. 2018;46(15):7772-92.
47. Timmons JA, Anighoro A, Brogan RJ, Stahl J, Wahlestedt C, Farquhar DG, et al. A human-based multi-gene signature enables quantitative drug repurposing for metabolic disease. eLife. 2022;11:e68832.
48. Fazakerley DJ, van Gerwen J, Cooke KC, Duan X, Needham EJ, Madsen S, et al. Phosphoproteomics reveals rewiring of the insulin signaling network and multi-nodal defects in insulin resistance. bioRxiv. 2022:2022.05.26.493198.
49. Timmers S, Konings E, Bilet L, Houtkooper RH, van de Weijer T, Goossens GH, et al. Calorie restriction-like effects of 30 days of resveratrol supplementation on energy metabolism and metabolic profile in obese humans. Cell Metab. 2011;14(5):612-22.
50. Knowler WC, Barrett-Connor E, Fowler SE, Hamman RF, Lachin JM, Walker EA, et al. Reduction in the incidence of type 2 diabetes with lifestyle intervention or metformin. N Engl J Med. 2002;346(6):393-403.
51. Geng L, Lam KSL, Xu A. The therapeutic potential of FGF21 in metabolic diseases: from bench to clinic. Nat Rev Endocrinol. 2020;16(11):654-67.
52. Bailly C. The bacterial thiopeptide thiostrepton. An update of its mode of action, pharmacological properties and applications. Eur J Pharmacol. 2022;914:174661.
53. Stöckli J, Davey JR, Hohnen-Behrens C, Xu A, James DE, Ramm G. Regulation of Glucose Transporter 4 Translocation by the Rab Guanosine Triphosphatase-Activating Protein AS160/TBC1D4: Role of Phosphorylation and Membrane Association. Molecular Endocrinology. 2008;22(12):2703-15.
54. Govers R, Coster ACF, James DE. Insulin increases cell surface GLUT4 levels by dose dependently discharging GLUT4 into a cell surface recycling pathway. Mol Cell Biol. 2004;24(14):6456-66.
55. Cho H, Mu J, Kim JK, Thorvaldsen JL, Chu Q, Crenshaw EB, 3rd, et al. Insulin resistance and a diabetes mellitus-like syndrome in mice lacking the protein kinase Akt2 (PKB beta). Science. 2001;292(5522):1728-31.
56. Hoehn KL, Hohnen-Behrens C, Cederberg A, Wu LE, Turner N, Yuasa T, et al. IRS1-independent defects define major nodes of insulin resistance. Cell Metab. 2008;7(5):421-33.
57. Hoy AJ, Brandon AE, Turner N, Watt MJ, Bruce CR, Cooney GJ, et al. Lipid and insulin infusion-induced skeletal muscle insulin resistance is likely due to metabolic feedback and not changes in IRS-1, Akt, or AS160 phosphorylation. Am J Physiol-Endoc M. 2009;297(1):E67-E75.
58. Cameron AR, Logie L, Patel K, Erhardt S, Bacon S, Middleton P, et al. Metformin selectively targets redox control of complex I energy transduction. Redox Biol. 2018;14:187-97.
59. Madiraju AK, Erion DM, Rahimi Y, Zhang XM, Braddock DT, Albright RA, et al. Metformin suppresses gluconeogenesis by inhibiting mitochondrial glycerophosphate dehydrogenase. Nature. 2014;510(7506):542-6.
60. Alexopoulos SJ, Chen S-Y, Brandon AE, Salamoun JM, Byrne FL, Garcia CJ, et al. Mitochondrial uncoupler BAM15 reverses diet-induced obesity and insulin resistance in mice. Nature Communications. 2020;11(1):2397.
61. Zhang L, Ging NC, Komoda T, Hanada T, Suzuki T, Watanabe K. Antibiotic susceptibility of mammalian mitochondrial translation. FEBS Lett. 2005;579(28):6423-7.
62. Weinhaeuser I, Pereira-Martins D, Hilberink JR, Ammatuna E, Huls GA, Rego EM, et al. Functional Drug Screen Identifies Thiostrepton, NAMPT Inhibitors and Metformin As Potential Candidates to Target the Macrophage Tumor Microenvironment in Acute Myeloid Leukemia. Blood. 2022;140(Supplement 1):8793-4.
63. Cunniff B, Newick K, Nelson KJ, Wozniak AN, Beuschel S, Leavitt B, et al. Disabling Mitochondrial Peroxide Metabolism via Combinatorial Targeting of Peroxiredoxin 3 as an Effective Therapeutic Approach for Malignant Mesothelioma. PLOS ONE. 2015;10(5):e0127310.

773 64. Hoehn KL, Salmon AB, Hohnen-Behrens C, Turner N, Hoy AJ, Maghzal GJ, et al. Insulin
774 resistance is a cellular antioxidant defense mechanism. Proceedings of the National Academy of
775 Sciences of the United States of America. 2009;106(42):17787-92.
776 65. Herzig S, Shaw RJ. AMPK: guardian of metabolism and mitochondrial homeostasis. Nat Rev
777 Mol Cell Biol. 2018;19(2):121-35.
778 66. Richter EA, Hargreaves M. Exercise, GLUT4, and skeletal muscle glucose uptake. Physiol Rev.
779 2013;93(3):993-1017.
780 67. Jensen TE, Schjerling P, Viollet B, Wojtaszewski JF, Richter EA. AMPK α1 activation is required
781 for stimulation of glucose uptake by twitch contraction, but not by H2O2, in mouse skeletal muscle.
782 PloS one. 2008;3(5).
783 68. Göransson O, McBride A, Hawley SA, Ross FA, Shpiro N, Foretz M, et al. Mechanism of action
784 of A-769662, a valuable tool for activation of AMP-activated protein kinase. J Biol Chem.
785 2007;282(45):32549-60.
786 69. Guo Q, Xu Z, Zhou D, Fu T, Wang W, Sun W, et al. Mitochondrial proteostasis stress in muscle
787 drives a long-range protective response to alleviate dietary obesity independently of ATF4. Sci Adv.
788 2022;8(30):eabo0340.
789 70. Hall C, Yu H, Choi E. Insulin receptor endocytosis in the pathophysiology of insulin resistance.
790 Exp Mol Med. 2020;52(6):911-20.
791 71. Lee J, Kim MS. The role of GSK3 in glucose homeostasis and the development of insulin
792 resistance. Diabetes Res Clin Pract. 2007;77 Suppl 1:S49-57.
793 72. Bernier M, Harney D, Koay YC, Diaz A, Singh A, Wahl D, et al. Elucidating the mechanisms by
794 which disulfiram protects against obesity and metabolic syndrome. npj Aging and Mechanisms of
795 Disease. 2020;6(1):8.
796 73. Bernier M, Mitchell SJ, Wahl D, Diaz A, Singh A, Seo W, et al. Disulfiram Treatment Normalizes
797 Body Weight in Obese Mice. Cell Metab. 2020;32(2):203-14.e4.
798 74. Gong L, Guo S, Zou Z. Resveratrol ameliorates metabolic disorders and insulin resistance in
799 high-fat diet-fed mice. Life Sci. 2020;242:117212.
800 75. Shu L, Hou G, Zhao H, Huang W, Song G, Ma H. Resveratrol improves high-fat diet-induced
801 insulin resistance in mice by downregulating the lncRNA NONMMUT008655.2. American journal of
802 translational research. 2020;12(1):1-18.
803 76. Rosales-Soto G, Diaz-Vegas A, Casas M, Contreras-Ferrat A, Jaimovich E. Fibroblast growth
804 factor-21 potentiates glucose transport in skeletal muscle fibers. Journal of Molecular Endocrinology.
805 2020;65(3):85-95.
806 77. Oost LJ, Kustermann M, Armani A, Blaauw B, Romanello V. Fibroblast growth factor 21
807 controls mitophagy and muscle mass. Journal of cachexia, sarcopenia and muscle. 2019;10(3):630-42.
808 78. Maier T, Güell M, Serrano L. Correlation of mRNA and protein in complex biological samples.
809 FEBS Lett. 2009;583(24):3966-73.
810 79. de Sousa Abreu R, Penalva LO, Marcotte EM, Vogel C. Global signatures of protein and mRNA
811 expression levels. Mol Biosyst. 2009;5(12):1512-26.
812 80. Gatti DM, Svenson KL, Shabalin A, Wu L-Y, Valdar W, Simecek P, et al. Quantitative Trait Locus
813 Mapping Methods for Diversity Outbred Mice. G3 Genes|Genomes|Genetics. 2014;4(9):1623-33.
814 81. Cavalli V, Vilbois F, Corti M, Marcote MJ, Tamura K, Karin M, et al. The stress-induced MAP
815 kinase p38 regulates endocytic trafficking via the GDI:Rab5 complex. Mol Cell. 2001;7(2):421-32.
816 82. Thompson JA, Carlson GM. The regulatory α and β subunits of phosphorylase kinase directly
817 interact with its substrate, glycogen phosphorylase. Biochem Biophys Res Commun. 2017;482(2):221-
818 5.
819 83. Polishchuk SV, Brandt NR, Meyer HE, Varsányi M, Heilmeyer LM, Jr. Does phosphorylase
820 kinase control glycogen biosynthesis in skeletal muscle? FEBS Lett. 1995;362(3):271-5.
821 84. Ding VW, Chen R-H, McCormick F. Differential regulation of glycogen synthase kinase 3β by
822 insulin and Wnt signaling. J Biol Chem. 2000;275(42):32475-81.

85. Skurat AV, Dietrich AD, Roach PJ. Interaction between glycogenin and glycogen synthase. Arch Biochem Biophys. 2006;456(1):93-7.
86. Trefely S, Khoo PS, Krycer JR, Chaudhuri R, Fazakerley DJ, Parker BL, et al. Kinome Screen Identifies PFKFB3 and Glucose Metabolism as Important Regulators of the Insulin/Insulin-like Growth Factor (IGF)-1 Signaling Pathway. J Biol Chem. 2015;290(43):25834-46.
87. Newick K, Cunniff B, Preston K, Held P, Arbiser J, Pass H, et al. Peroxiredoxin 3 is a redox-dependent target of thiostrepton in malignant mesothelioma cells. PLoS One. 2012;7(6):e39404.
88. Liu J, Wen D, Fang X, Wang X, Liu T, Zhu J. p38MAPK Signaling Enhances Glycolysis Through the Up-Regulation of the Glucose Transporter GLUT-4 in Gastric Cancer Cells. Cell Physiol Biochem. 2015;36(1):155-65.
89. Kulisz A, Chen N, Chandel NS, Shao Z, Schumacker PT. Mitochondrial ROS initiate phosphorylation of p38 MAP kinase during hypoxia in cardiomyocytes. Am J Physiol Lung Cell Mol Physiol. 2002;282(6):L1324-9.
90. Wang F, Qi XM, Wertz R, Mortensen M, Hagen C, Evans J, et al. p38γ MAPK Is Essential for Aerobic Glycolysis and Pancreatic Tumorigenesis. Cancer Res. 2020;80(16):3251-64.
91. Liu L, Cui J, Zhao Y, Liu X, Chen L, Xia Y, et al. KDM6A-ARHGDIB axis blocks metastasis of bladder cancer by inhibiting Rac1. Mol Cancer. 2021;20(1):77.
92. Gee HY, Saisawat P, Ashraf S, Hurd TW, Vega-Warner V, Fang H, et al. ARHGDIA mutations cause nephrotic syndrome via defective RHO GTPase signaling. J Clin Invest. 2013;123(8):3243-53.
93. Sylow L, Jensen TE, Kleinert M, Højlund K, Kiens B, Wojtaszewski J, et al. Rac1 signaling is required for insulin-stimulated glucose uptake and is dysregulated in insulin-resistant murine and human skeletal muscle. Diabetes. 2013;62(6):1865-75.
94. Chesler EJ, Gatti DM, Morgan AP, Strobel M, Trepanier L, Oberbeck D, et al. Diversity Outbred Mice at 21: Maintaining Allelic Variation in the Face of Selection. G3 (Bethesda, Md). 2016;6(12):3893-902.
95. Morgan AP, Fu CP, Kao CY, Welsh CE, Didion JP, Yadgary L, et al. The Mouse Universal Genotyping Array: From Substrains to Subspecies. G3 (Bethesda, Md). 2015;6(2):263-79.
96. Broman KW, Gatti DM, Svenson KL, Sen Ś, Churchill GA. Cleaning Genotype Data from Diversity Outbred Mice. G3 Genes|Genomes|Genetics. 2019;9(5):1571-9.
97. Frezza C, Cipolat S, Scorrano L. Organelle isolation: functional mitochondria from mouse liver, muscle and cultured filroblasts. Nat Protoc. 2007;2(2):287-95.
98. Acin-Perez R, Benador IY, Petcherski A, Veliova M, Benavides GA, Lagarrigue S, et al. A novel approach to measure mitochondrial respiration in frozen biological samples. The EMBO Journal. 2020;39(13):e104073.
99. Rappsilber J, Mann M, Ishihama Y. Protocol for micro-purification, enrichment, pre-fractionation and storage of peptides for proteomics using StageTips. Nat Protoc. 2007;2(8):1896-906.
100. Demichev V, Messner CB, Vernardis SI, Lilley KS, Ralser M. DIA-NN: neural networks and interference correction enable deep proteome coverage in high throughput. Nat Methods. 2020;17(1):41-4.
101. Perez-Riverol Y, Bai J, Bandla C, García-Seisdedos D, Hewapathirana S, Kamatchinathan S, et al. The PRIDE database resources in 2022: a hub for mass spectrometry-based proteomics evidences. Nucleic Acids Res. 2022;50(D1):D543-d52.
102. R Core Team R. R: A language and environment for statistical computing. 2013.
103. Dabney A, Storey JD, Warnes GJRpv. qvalue: Q-value estimation for false discovery rate control. 2010;1(0).
104. Yu G, Wang L-G, Han Y, He Q-YJOajoib. clusterProfiler: an R package for comparing biological themes among gene clusters. 2012;16(5):284-7.
105. Liao Y, Wang J, Jaehnig EJ, Shi Z, Zhang B. WebGestalt 2019: gene set analysis toolkit with revamped UIs and APIs. Nucleic Acids Res. 2019;47(W1):W199-w205.

872 106. Broman KW, Gatti DM, Simecek P, Furlotte NA, Prins P, Sen Ś, et al. R/qtl2: Software for
873 Mapping Quantitative Trait Loci with High-Dimensional Data and Multiparent Populations. Genetics.
874 2019;211(2):495-502.
875 107. Stegle O, Parts L, Piipari M, Winn J, Durbin R. Using probabilistic estimation of expression
876 residuals (PEER) to obtain increased power and interpretability of gene expression analyses. Nat
877 Protoc. 2012;7(3):500-7.
878 108. Carey AL, Steinberg GR, Macaulay SL, Thomas WG, Holmes AG, Ramm G, et al. Interleukin-6
879 increases insulin-stimulated glucose disposal in humans and glucose uptake and fatty acid oxidation
880 in vitro via AMP-activated protein kinase. Diabetes. 2006;55(10):2688-97.
881 109. Masson SWC, Sorrenson B, Shepherd PR, Merry TL. beta-catenin regulates muscle glucose
882 transport via actin remodelling and M-cadherin binding. Mol Metab. 2020;42:101091.
883 110. Schneider CA, Rasband WS, Eliceiri KW. NIH Image to ImageJ: 25 years of image analysis. Nat
884 Methods. 2012;9(7):671-5.
885 111. Yau B, Naghiloo S, Diaz-Vegas A, Carr AV, Van Gerwen J, Needham EJ, et al. Proteomic
886 pathways to metabolic disease and type 2 diabetes in the pancreatic islet. iScience.
887 2021;24(10):103099.

888

889

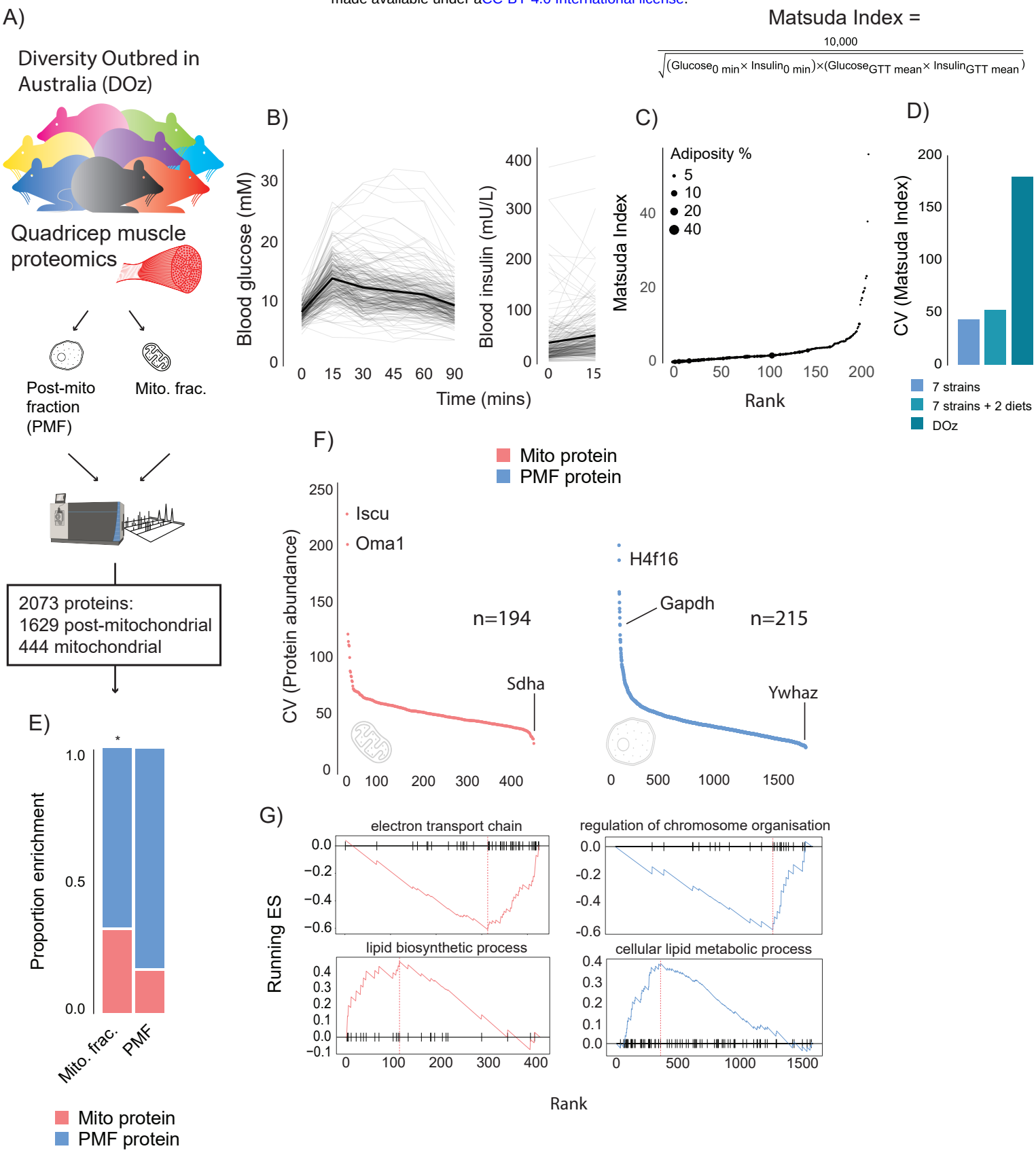

Figure 2

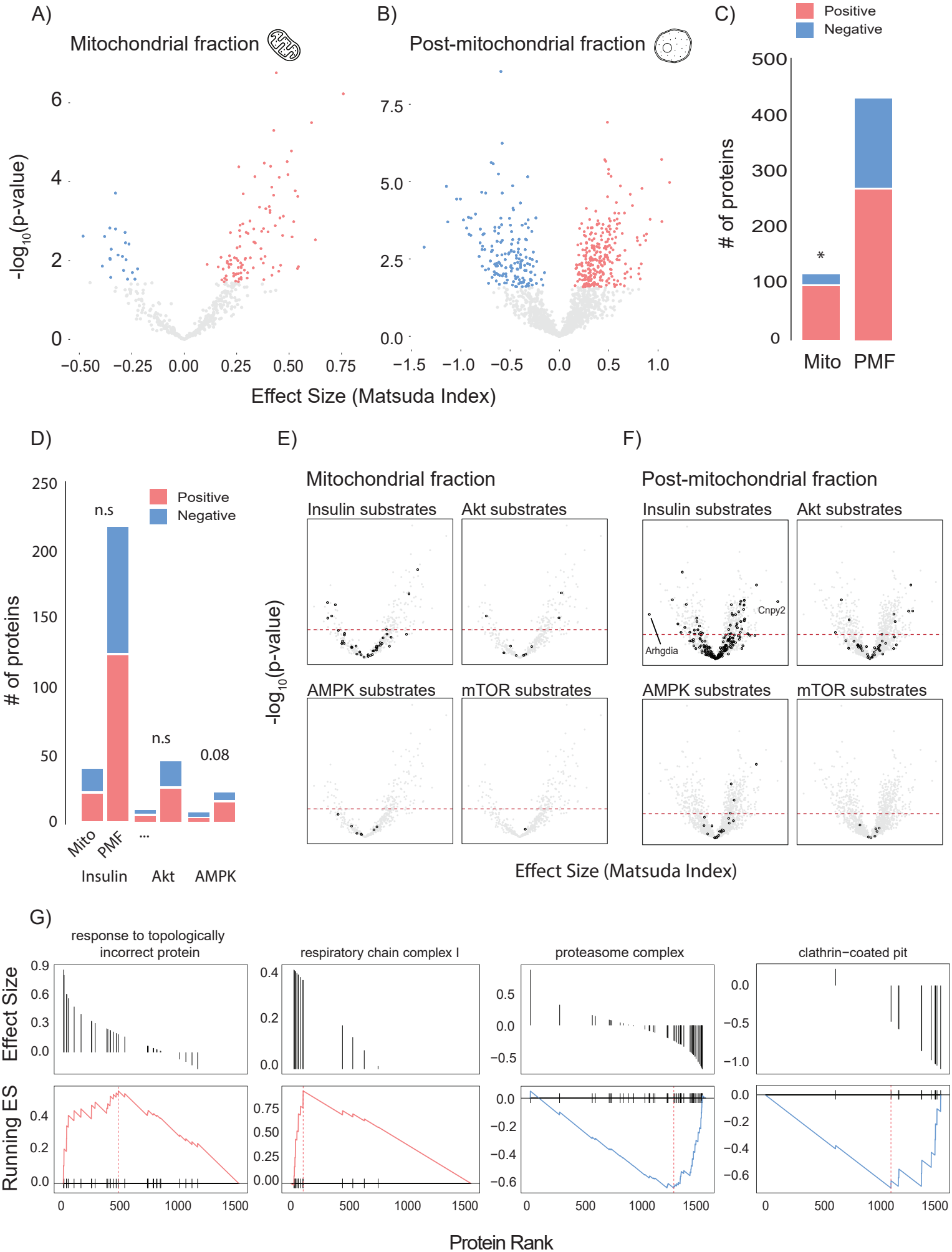

Figure 3:

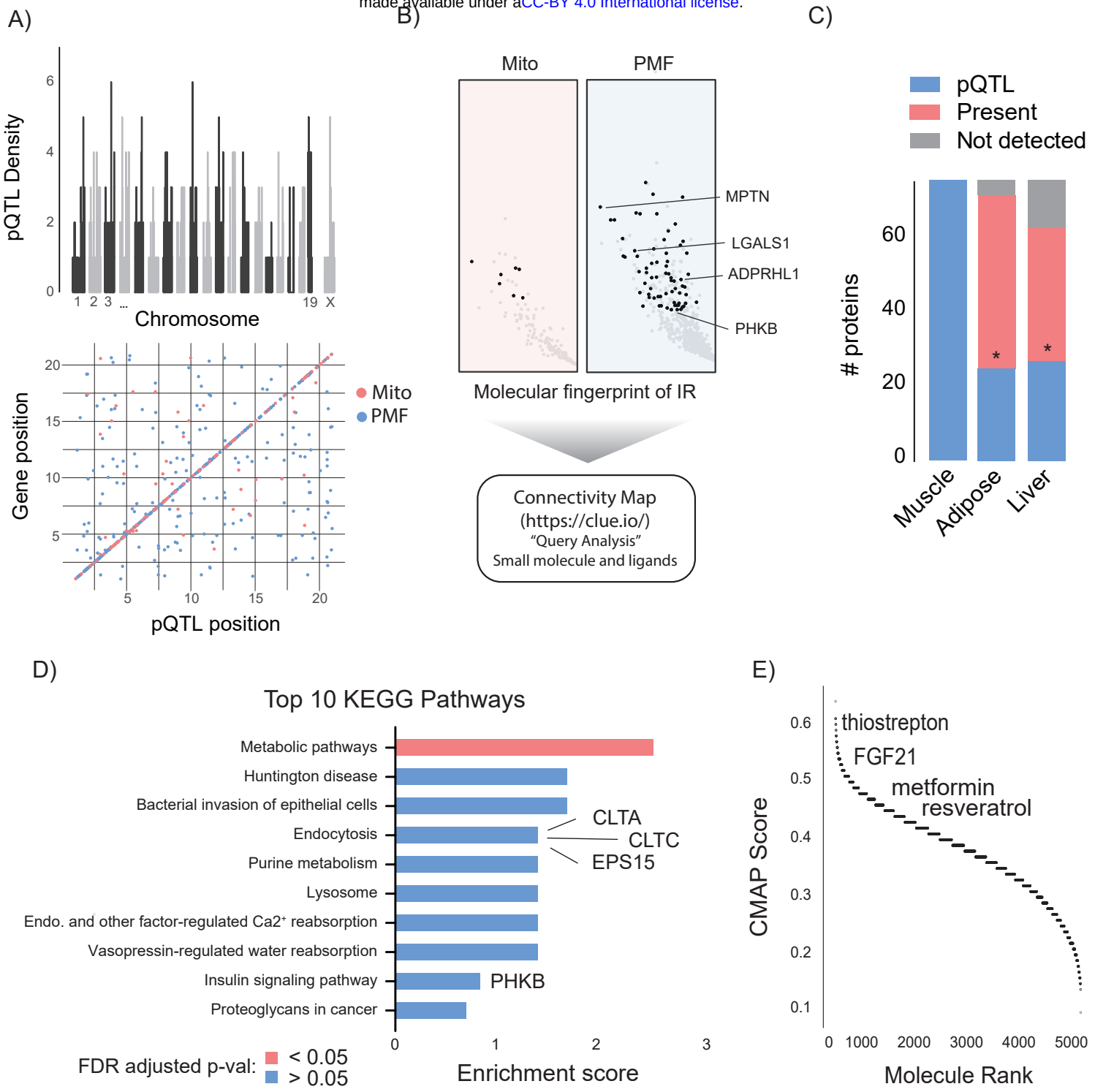

Figure 4

A)

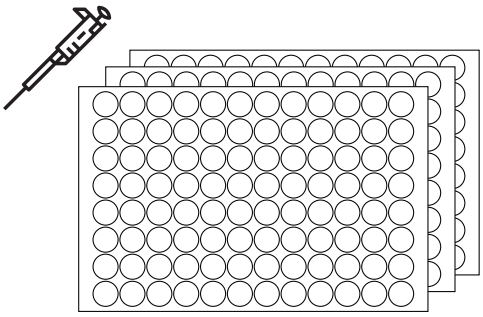

B)

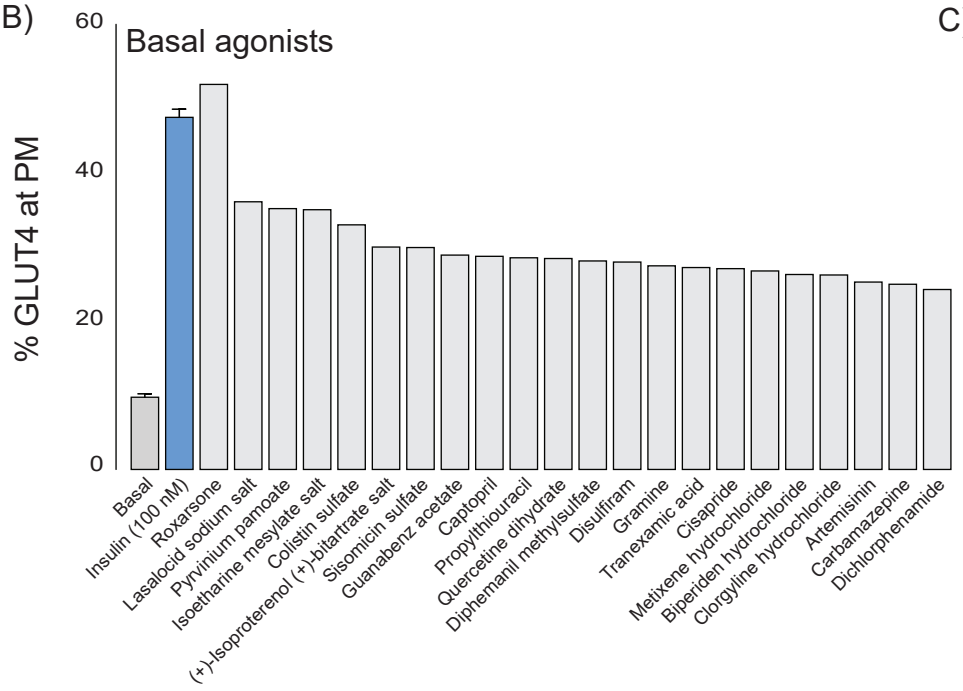

C)

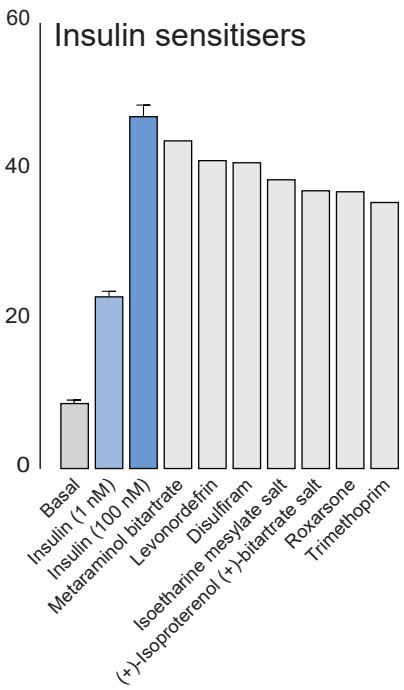

D)

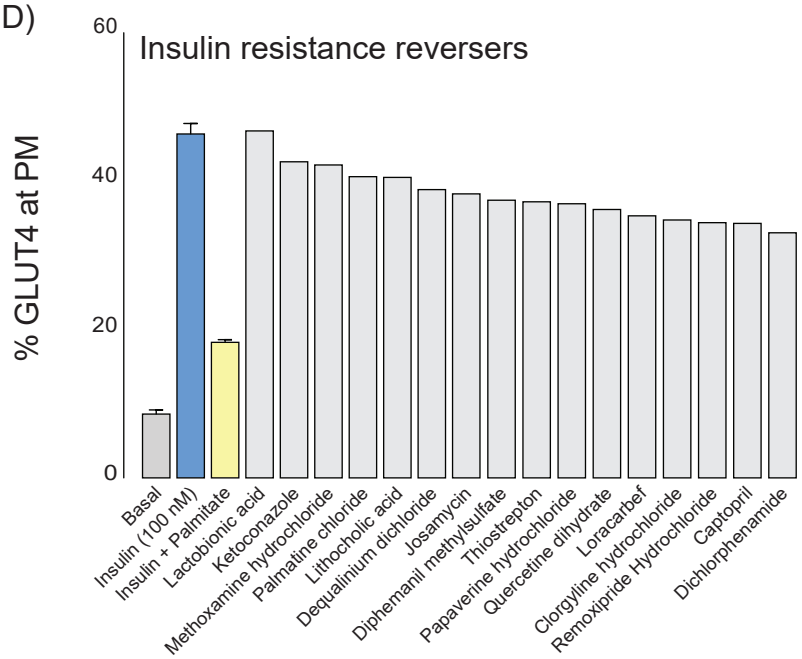

E)

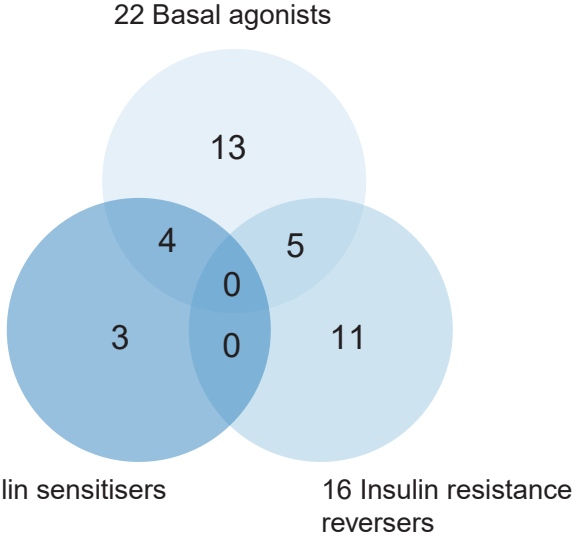

Figure 5.

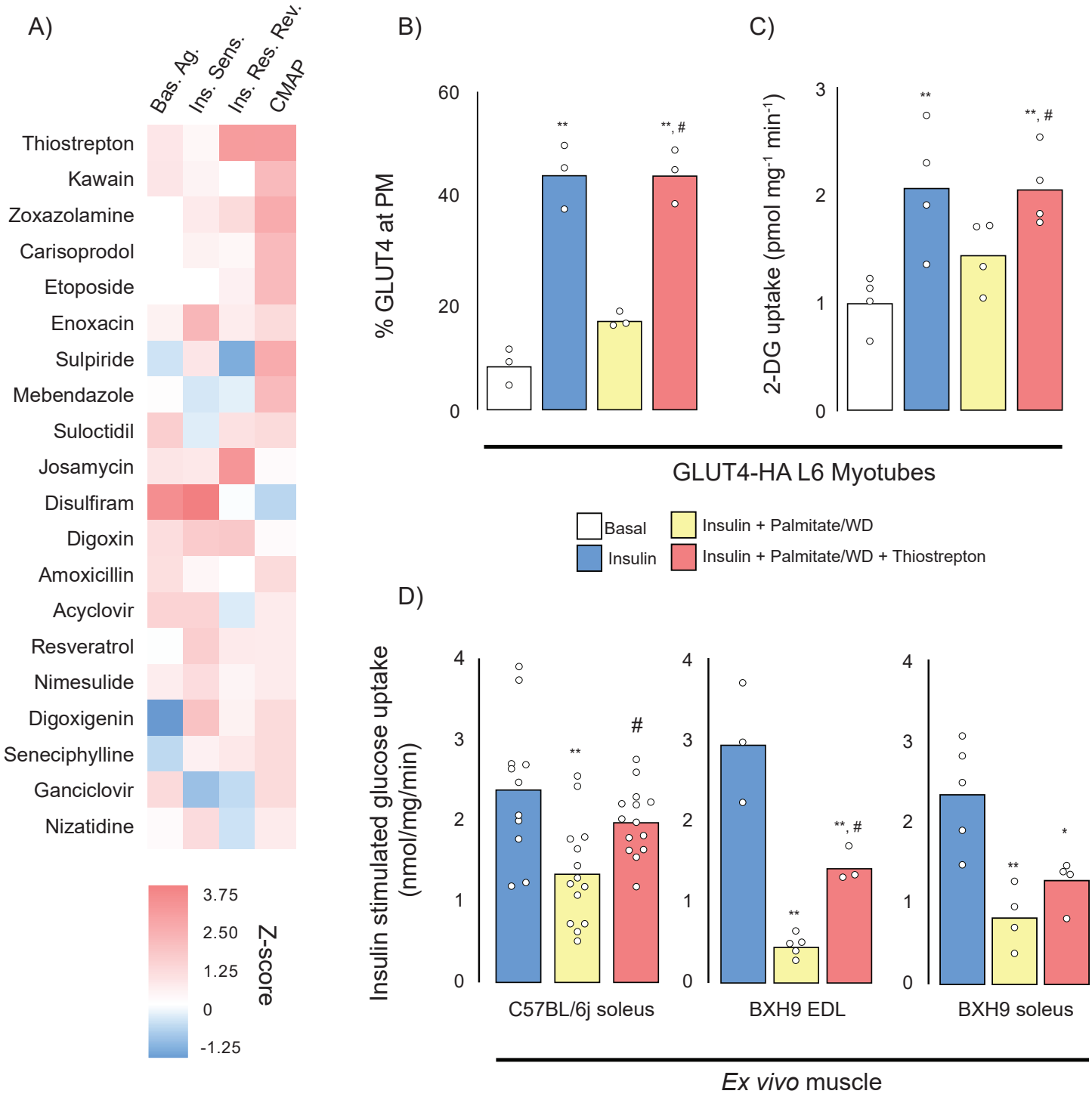

Figure 6

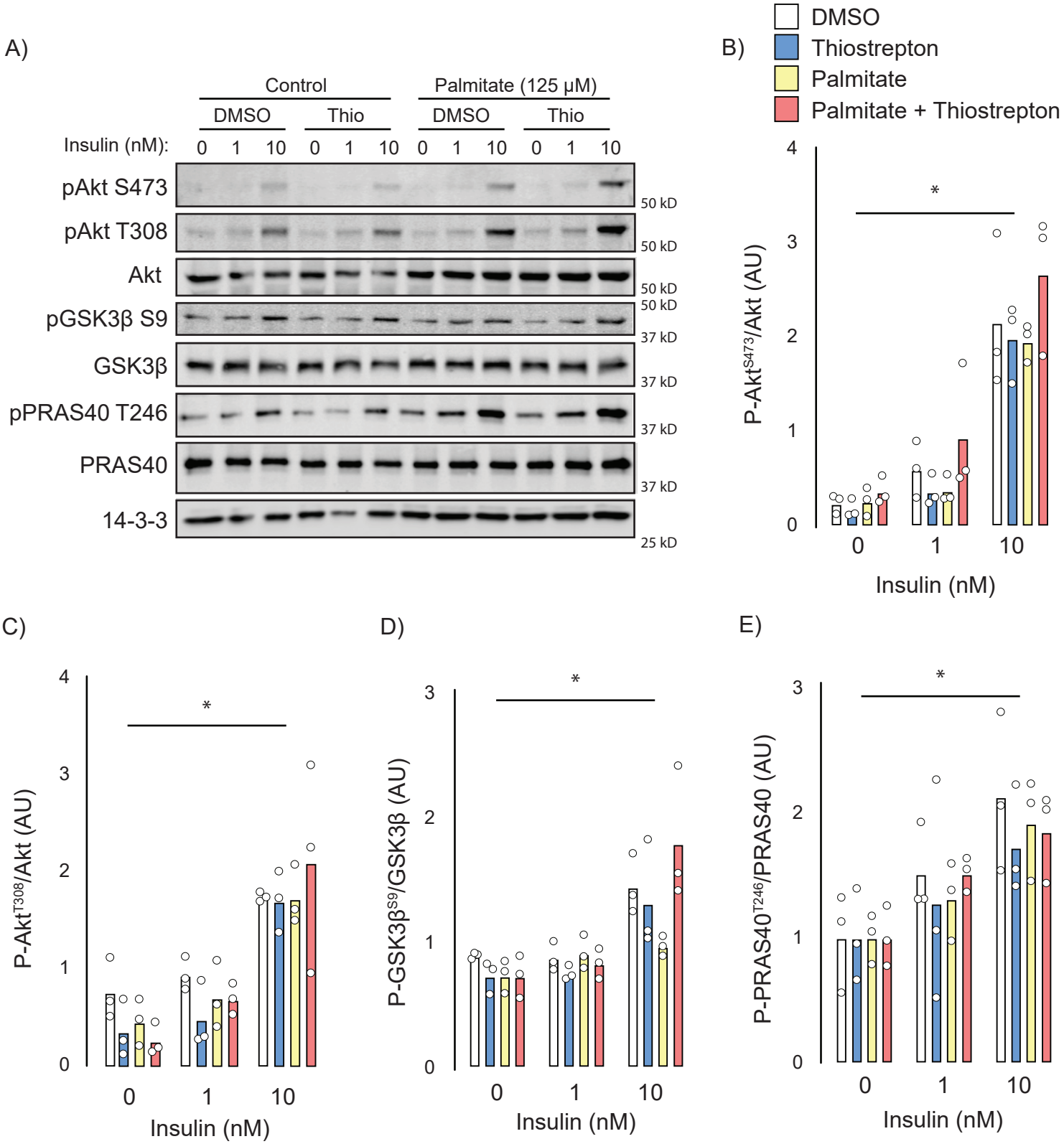

Figure 7

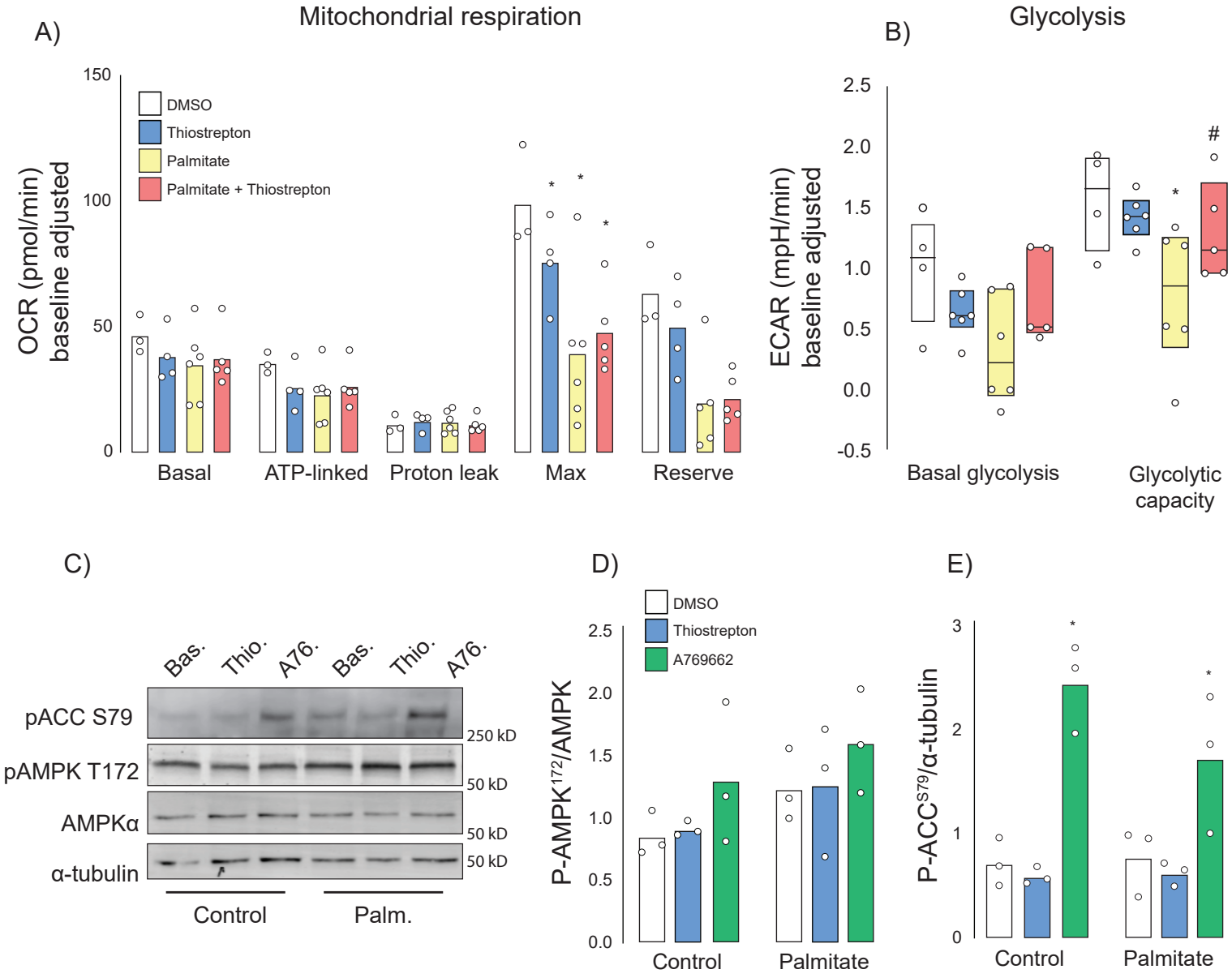

Supplementary Figure 1:

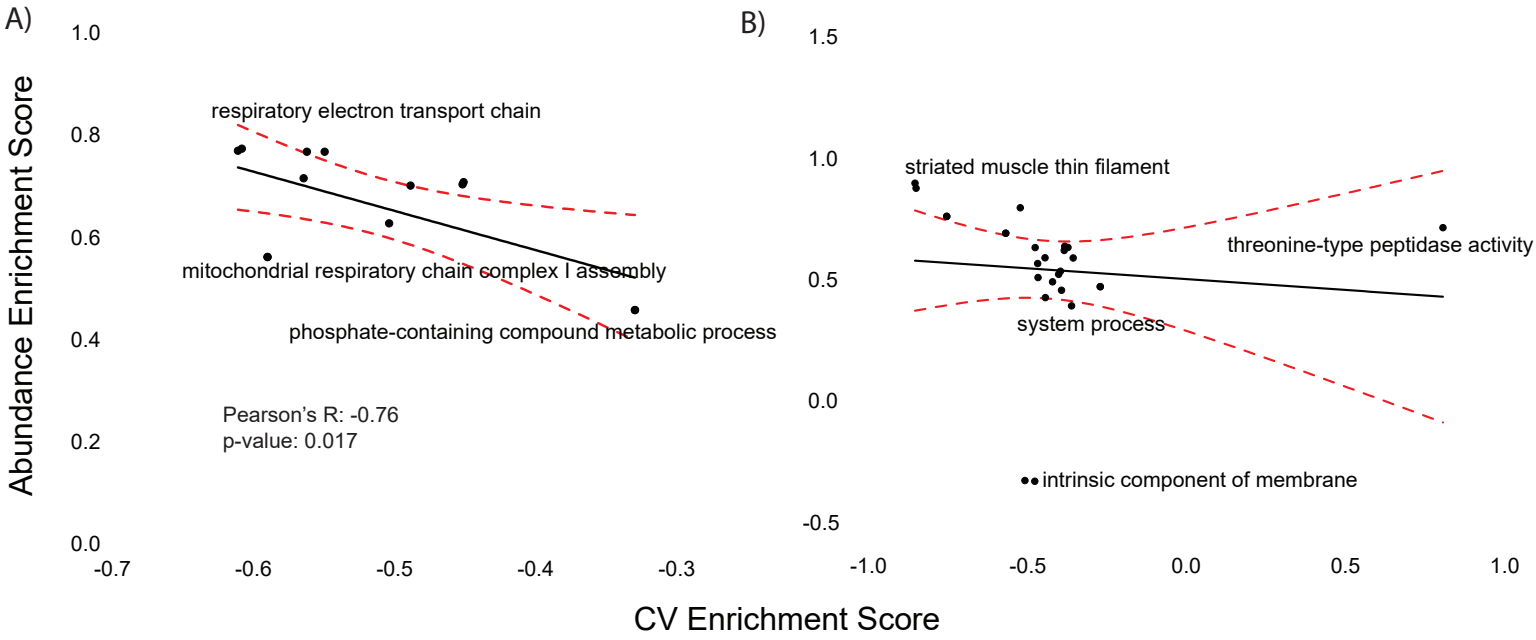

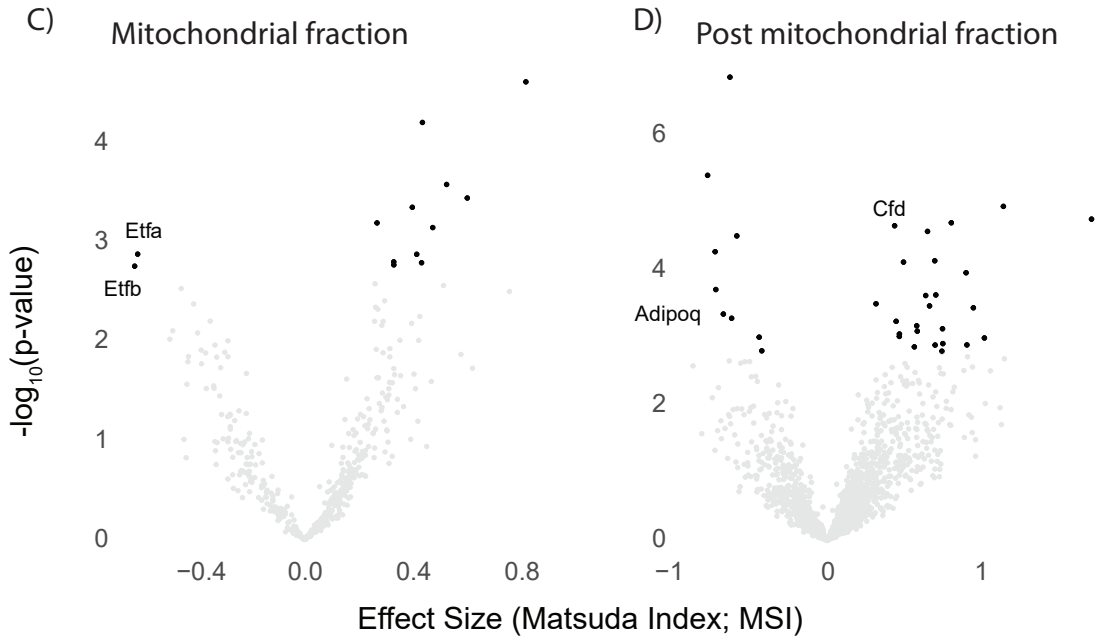

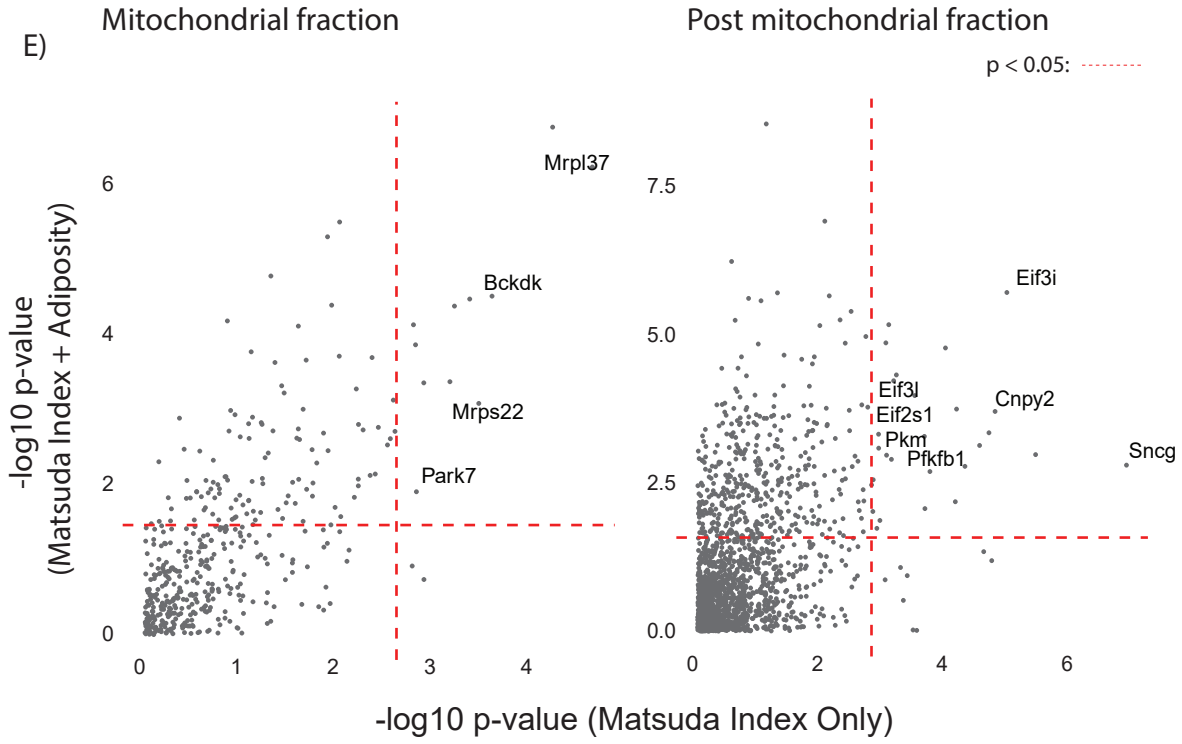

Supplementary Figure 2.

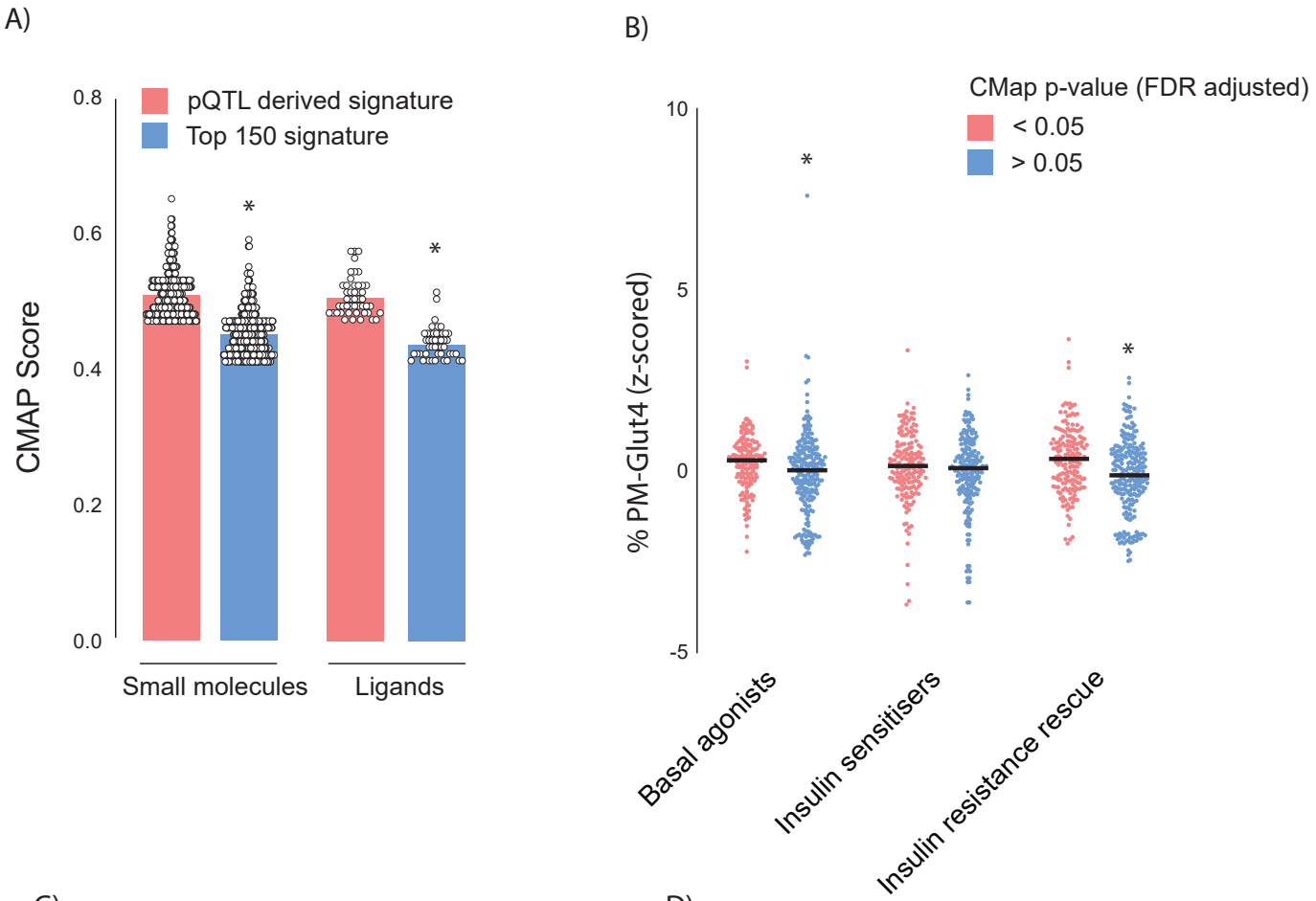

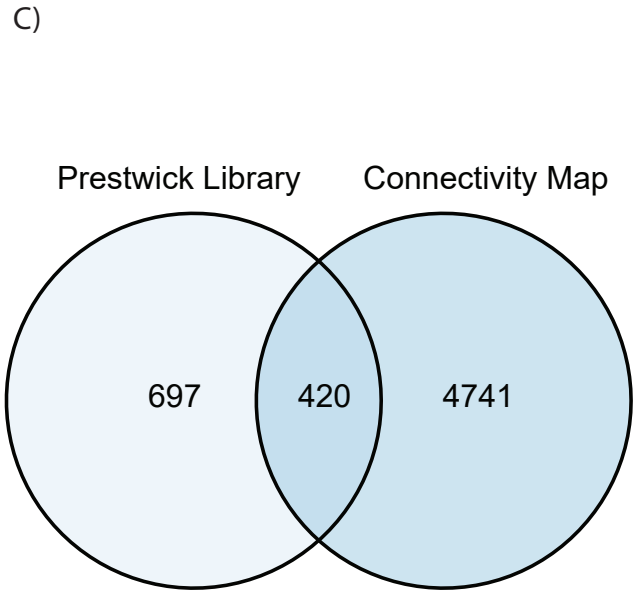

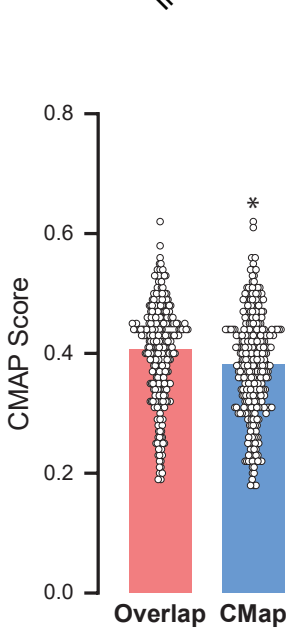

Supplementary Figure 3:

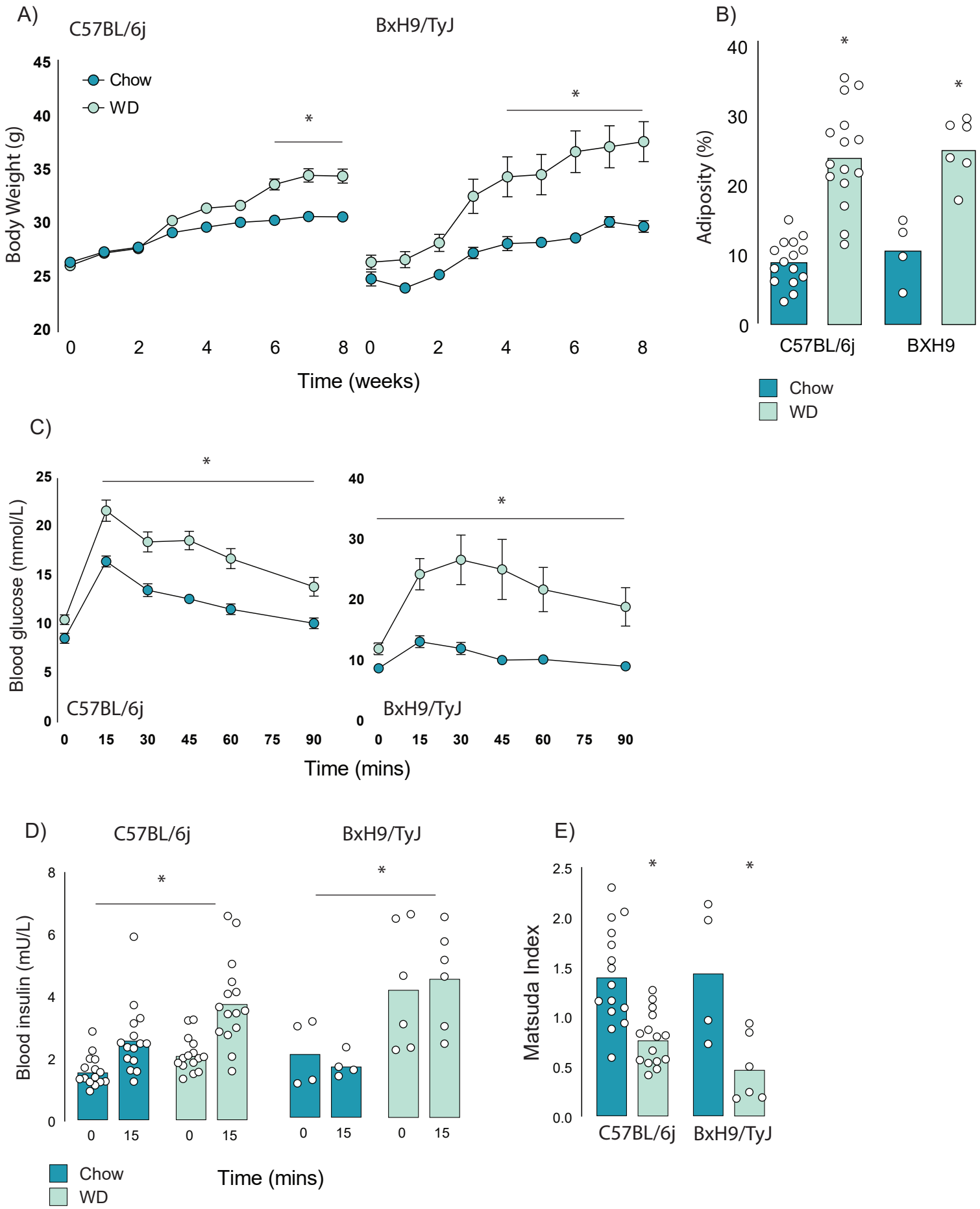

890 Figure Legends

891 Figure 1. Metabolic and proteomic diversity of Diversity Outbred in Oz (DOz) mice. (A) Schematic of
892 metabolic phenotyping and quadricep proteomics in chow fed DOz mice. (B) Blood glucose and insulin
893 levels during a GTT. (C) Whole-body insulin sensitivity (Matsuda Index, formula shown above) and
894 adiposity of DOz mice (n= 215). (D) Comparison of coefficient of variation (CV) of insulin of Matsuda
895 Index across inbred strains and diets versus chow fed DOz mice. (E) Relative enrichment of
896 mitochondrial (Mito) proteins in mitochondrial fraction and post-mitochondrial fraction (PMF) of
897 quadricep proteomes. (F) Relative protein CV across mitochondrial and post-mitochondrial quadricep
898 fractions. (G) Biological pathways enriched in mitochondrial and post-mitochondrial quadricep
899 fractions, running enrichment score for a given pathway (ES) on y-axis and proteins ranked by CV on
900 x-axis. Significance testing was performed by Chi-square test. * Indicates a significant difference $P <$
901 0.01.

902

903 Figure 2. Linear modelling of quadricep proteome and whole-body insulin sensitivity. (A-B) Volcano
904 plot with Matsuda Index effect sizes (x-axis) and significance (y-axis) for mitochondrial (A) and post-
905 mitochondrial (B) quadricep proteins using a linear model with adiposity as a covariate. Significant
906 proteins with positive and negative effect sizes are indicated in red and blue, respectively. (C)
907 Comparison of positively and negatively associated proteins between fractions. (D) Number of
908 proteins identified in each fraction with known roles in insulin or AMPK signalling. (E-F) Volcano plot
909 shown in A with mitochondrial (E) and post-mitochondrial fraction (F) proteins shown in black that
910 have documented roles in indicated signalling pathways. Adjusted p-value threshold is indicated (red
911 dotted line). (G) Pathways enriched for proteins which positively and negative associate with Matsuda
912 Index. Effect sizes of proteins within a given pathway and running enrichment score (ES) for a that
913 pathway on y-axis and proteins ranked by CV on x-axis. (ES) on y-axis and proteins ranked by CV on x-
914 axis. of proteins within pathways that are enriched for proteins associated with whole-body insulin

915 sensitivity. Proteins ranked by Matsuda Index effect size on x-axis. Linear modelling was performed
916 using a gaussian distribution with q-value adjustment of p-values. Enrichment tests between fractions
917 were performed by Chi-square test. * Indicates a significant difference $P < 0.01$.

918

919 Figure 3. Integration of proteomic data via Connectivity Map. (A-B) Workflow includes filtering for
920 proteins with cis-pQTL (A) and negative association with Matsuda Index (B) prior to Connectivity Map
921 query. (A) Distribution of cis and trans-pQTL across mitochondrial and PMF proteome. (B) Left side of
922 volcano plots from Figure 2A-B (proteins negatively associated with Matsuda Index) is shown with
923 proteins comprised in Molecular Fingerprint of insulin resistance (IR) indicated in black. Proteins with
924 human homologues are highlighted. (C) Comparison of Molecular Fingerprint of insulin resistance
925 across muscle adipose and liver proteomes. (D) Top 10 KEGG pathways enriched in the molecular
926 fingerprint of insulin resistance with proteins of interest highlighted. (E) Distribution of Connectivity
927 Map (CMAP) scores for identified small molecules and ligands with compounds of interest indicated.
928 Significance testing was performed by Chi-square test. * Indicates a significant difference $P < 0.001$.

929

930 Figure 4. Prestwick library of FDA-approved drugs that modulate GLUT4 translocation in L6 myotubes.
931 (A) Schematic representation of the three assays performed. (B) Small molecules that promote GLUT4
932 exocytosis to the plasma membrane independently of insulin with controls (Basal, Insulin) on the left.
933 (C) Small molecules that potentiate a submaximal dose of insulin (1 nM) with controls (Basal, 1 nM
934 and 100 nM Insulin) on the left. Compounds were added in combination with 1 nM insulin. (D) Small
935 molecules that reverse palmitate induced insulin resistance with controls (Basal, Insulin, Insulin +
936 Palmitate) on the left. Compounds were added in combination with 100 nM insulin following palmitate
937 treatment. (E) Venn diagram of compound overlap between assays. Biological significance for each
938 assay was defined as 50% of corresponding control, see methods for details. Plasma-membrane; PM.

939

940 Figure 5. Cross-validation of Connectivity Map and Prestwick library. (A) Scoring matrix of top 20
941 scoring compounds present in both Connectivity Map (CMAP) and the Prestwick library screens (Basal
942 Agonists, Bas.Ag.; Insulin Sensitizer, Ins. Sens; Insulin Resistance Reversers, Ins. Res. Rev). (B-C) Insulin
943 stimulated GLUT4 translocation to the plasma membrane (PM, B) and 2-deoxyglucose uptake (C) in
944 control and insulin resistant L6 myotubes (Palmitate) treated with thiostrepton or vehicle control. (D)
945 Insulin stimulated 2-deoxyglucose uptake in soleus and extensor digitorum longus (EDL) muscles from
946 chow and WD fed C57BL/6J and BXH9/TyJ following ex vivo treatment with thiostrepton or vehicle
947 control. Data are mean with individual data points shown, n=3-4 (B-C), n=3-5 (BXH9) n=11-14
948 (C57BL/6J). Significance was determined by one-way ANOVA with Student's post hoc test. ** Indicates
949 significant difference from control (Basal or chow fed C57BL6/J) group ($p < 0.01$), * Indicates significant
950 difference from control ($p < 0.05$). # Indicates significant difference from palmitate-treated or WD-fed
951 fed control group ($p < 0.05$).

952

953 Figure 6. Effect of thiostrepton on insulin signalling. (A-E) Immunoblotting with indicated antibodies
954 of control and palmitate treated GLUT4-HA-L6 myotubes following treatment with thiostrepton or
955 vehicle control and stimulation with 0, 1, or 10 nM insulin. (A) Representative immunoblot shown of
956 3 independent experiments. (B-E) Quantification of immunoblots in A, Akt S473 (B), Akt T308 (C),
957 GSK3β S9 (D) and PRAS40 T246 (E). Data are mean with individual data points, n=3. Significance was
958 determined by two-way ANOVA with Student's post hoc test. * Indicates a significant effect of insulin
959 $P < 0.01$.

960

961 Figure 7. Effect of thiostrepton on mitochondrial respiration and glycolysis. (A-B) Oxygen consumption
962 rates (A) and extracellular acidification rates (B) in control and palmitate treated GLUT4-HA-L6

963 myotubes treated with either thiostrepton or vehicle control. (C) Immunoblotting of AMPK signalling
964 in control and palmitate treated (Palm.) GLUT4-HA-L6 myotubes treated with either thiostrepton
965 (Thio.), vehicle control (Bas.) or positive control A-769662 (A76.). Representative immunoblots shown
966 of 3 independent experiments. (D-E) Quantification of immunoblots in C, AMPK T172 (D) and ACC S79
967 (E) phosphorylation following thiostrepton or A-769662 treatment. Data are mean with individual data
968 points shown, n=3. * Indicates significant difference from control cells, # indicates significant
969 difference from palmitate treated cells $p < 0.05$.

970

971 Supplementary Figure 1. Comparison of enrichment analysis and linear modelling approaches for DOz
972 insulin sensitivity and muscle proteomics. (A-B) Abundance (y-axis) and coefficient of variation-based
973 (x-axis) gene-ontology enrichment scores for mitochondrial (A) and PMF (B) proteomes. (C-D) Volcano
974 plot with Matsuda Index effect sizes (x-axis) and significance (y-axis) for mitochondrial (C) and post-
975 mitochondrial fraction (D) proteins. (E-F) Mitochondrial (E) and post-mitochondrial fraction (F)
976 negative log10 p-values for Matsuda Index effect sizes from linear models with and without adiposity
977 as a covariate. Dashed red line indicates FDR adjusted $p < 0.05$.

978

979 Supplementary Figure 2. Evaluation of Connectivity Map analysis. (A) Raw Connectivity Map (CMAP)
980 scores for compounds and ligands identified by Connectivity map using either a pQTL filtered signature
981 (Fingerprint) or a signature of the 150 proteins with the largest negative effect sizes. (B) Comparison
982 of z scored GLUT4 at plasma membrane (PM) after treatment with Prestwick library compounds based
983 on CMAP significance. (C) Overlap of compounds found in both the Prestwick library and Connectivity
984 Map. (D) Comparison of Connectivity Map scores between overlapping compounds and all of
985 Connectivity Map. Data are mean with individual data points. Significance was determined by two-
986 way ANOVA with Student's post hoc test or Student's t-test. * Indicates a significant difference
987 between groups $P < 0.01$.

Supplementary Figure 3. Effect of western diet feeding on C57BL/6J and BxH9/TyJ mice body composition and insulin sensitivity. (A-E) Body weights (A), adiposity (B), blood glucose (C) and insulin (D) during a glucose tolerance test, and Matsuda Index (E) of C57BL/6J and BxH9/TyJ mice fed a chow of high-fat/high-sugar (western diet; WD) for 8 weeks. Data are mean with individual data points, n= 4-6 (BxH9), n=15 (C57BL/6J).

Supplementary Table 1. List of proteins and their Matsuda Index effect sizes which comprise our pQTL-filtered molecular fingerprint of insulin resistance.

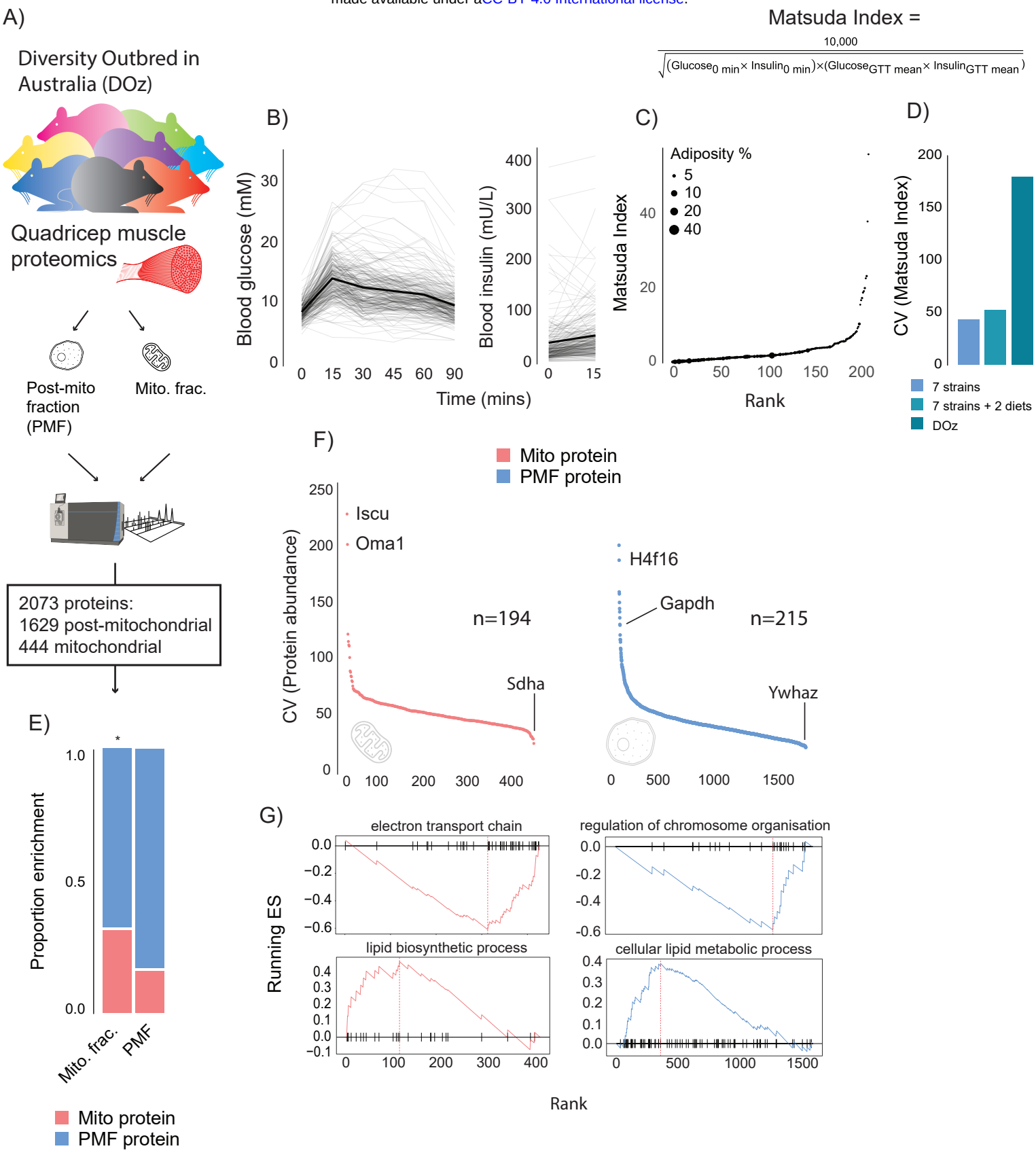

Figure 2

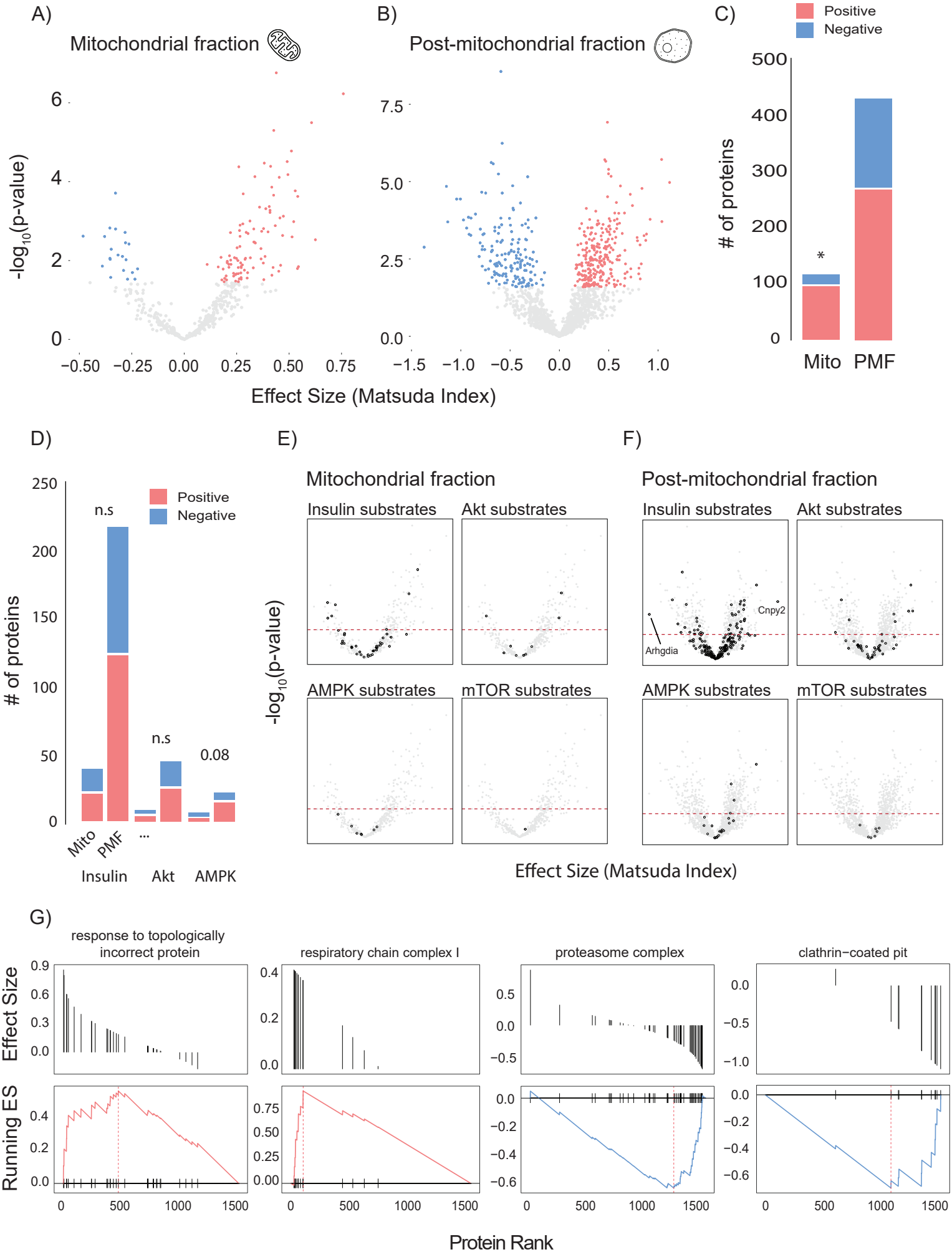

Figure 3:

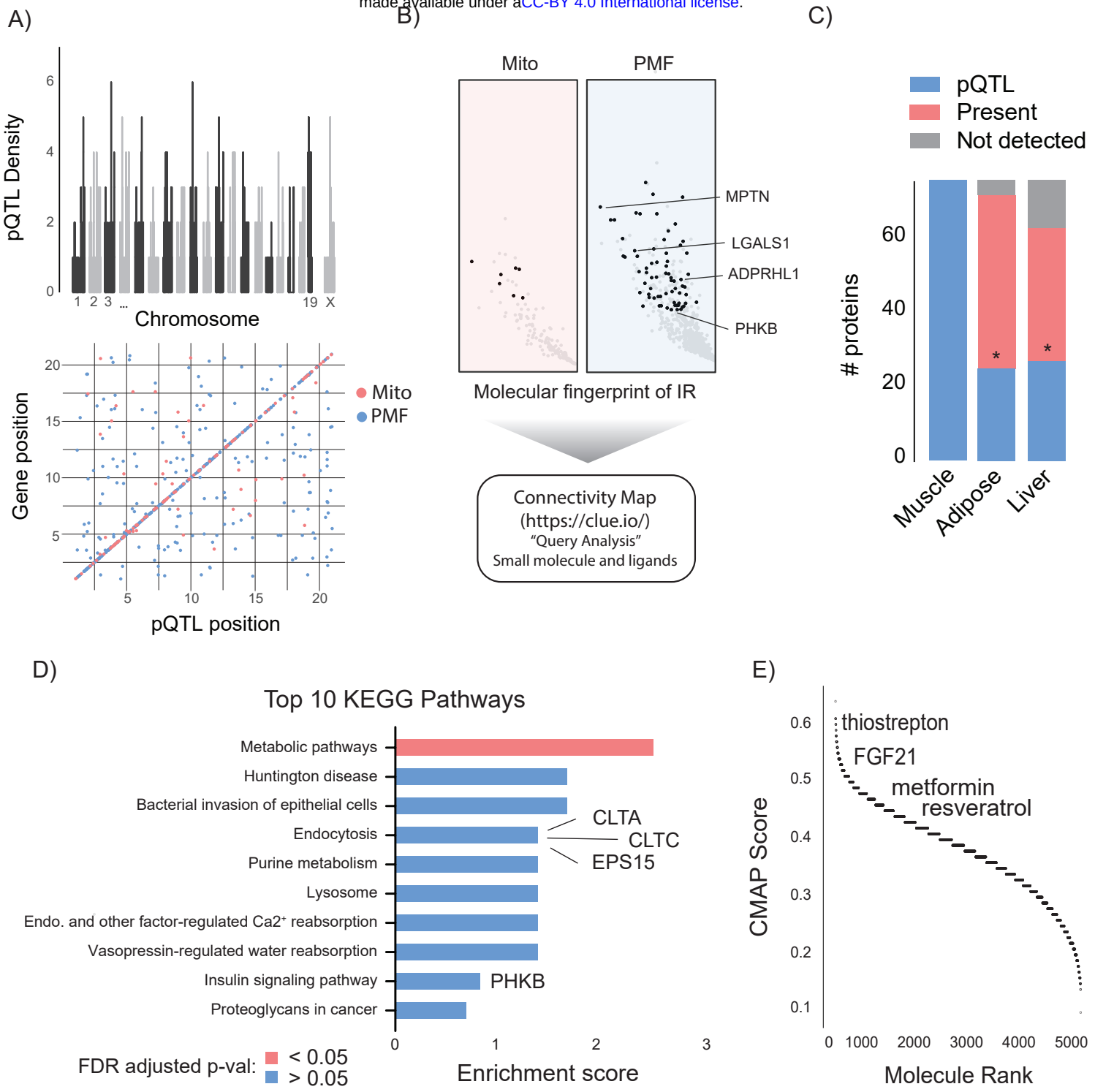

Figure 4

A)

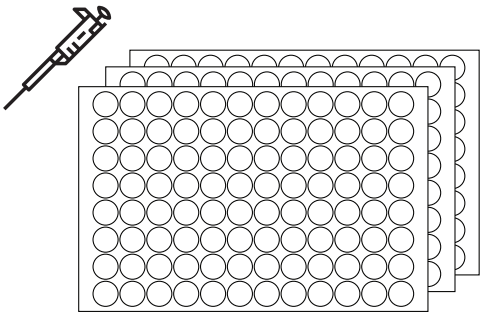

B)

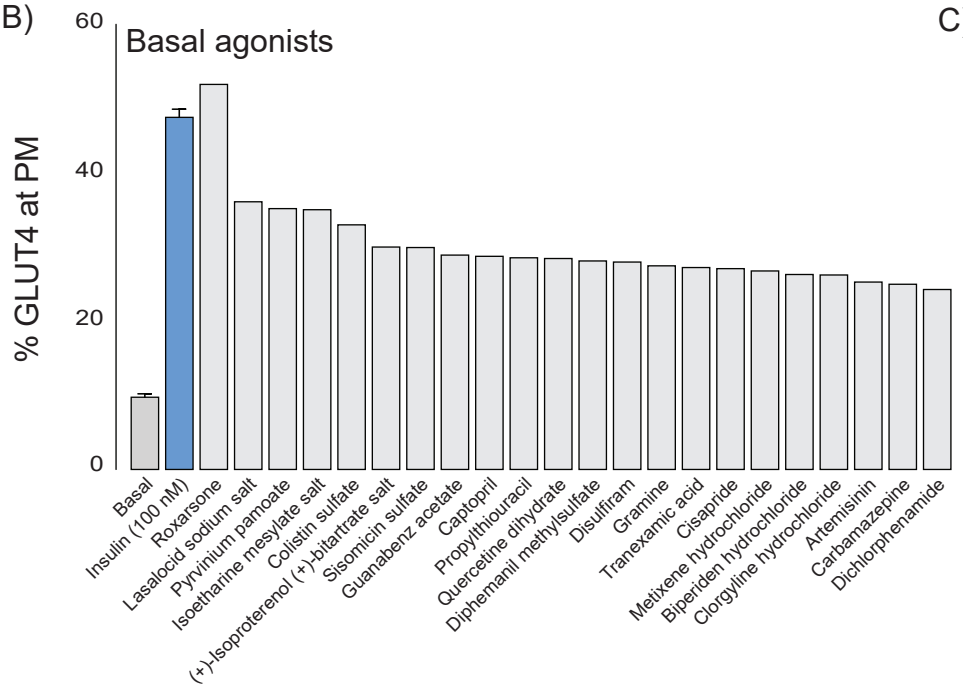

C)

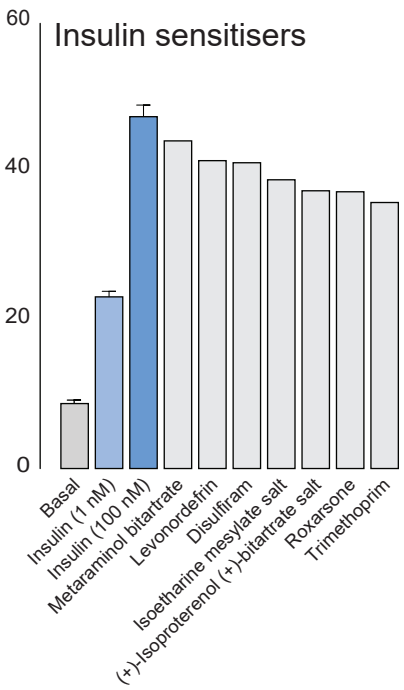

D)

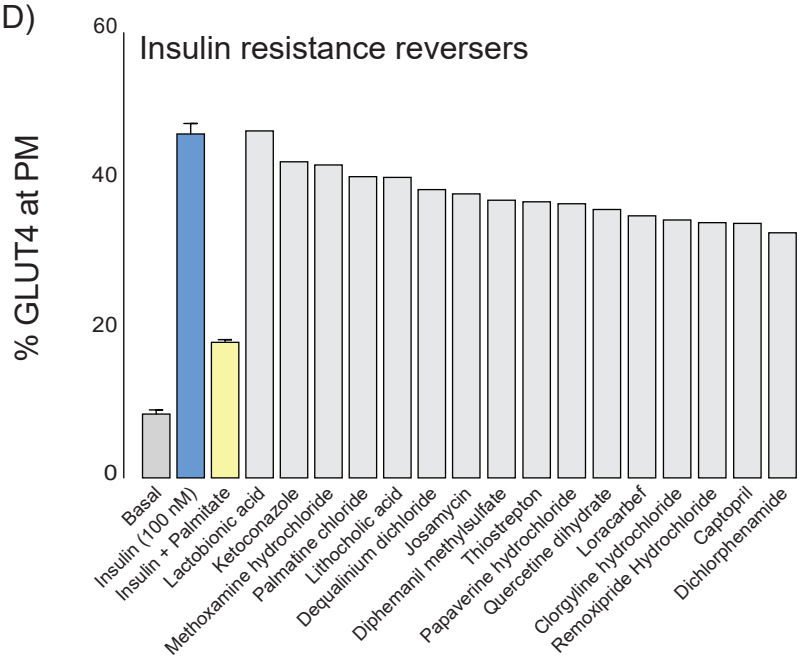

E)

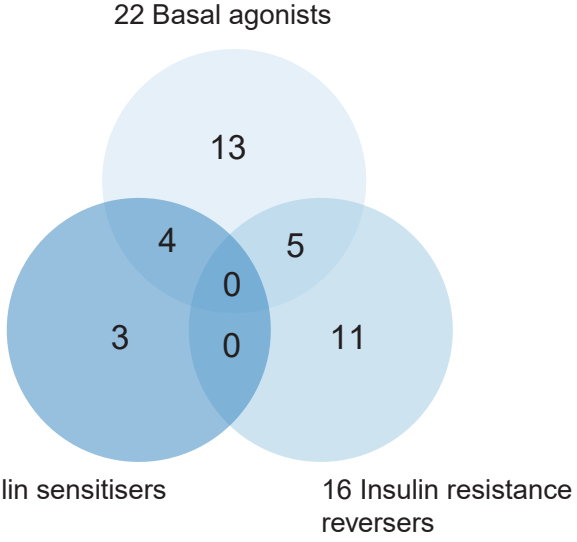

Figure 5.

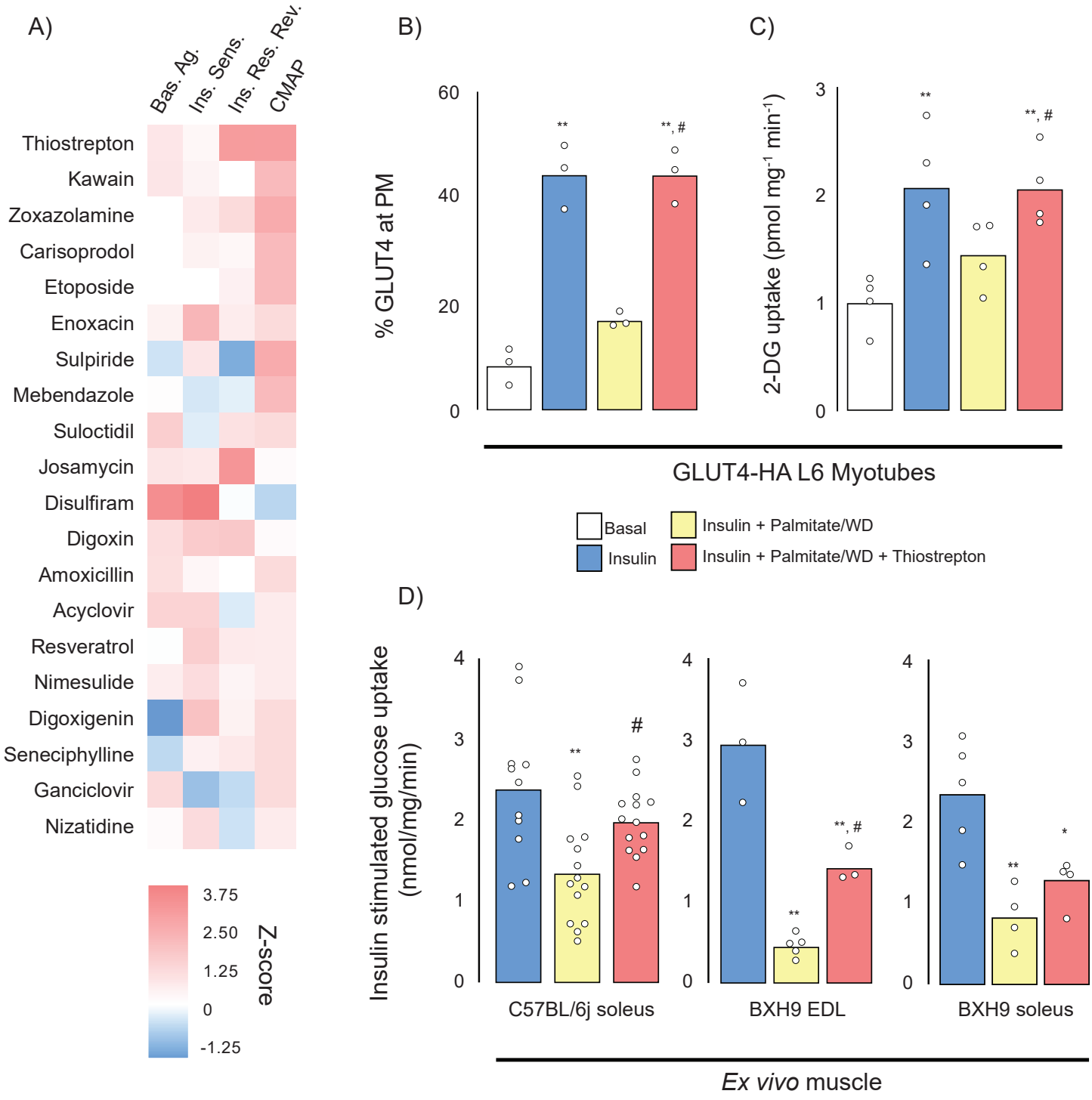

Figure 6

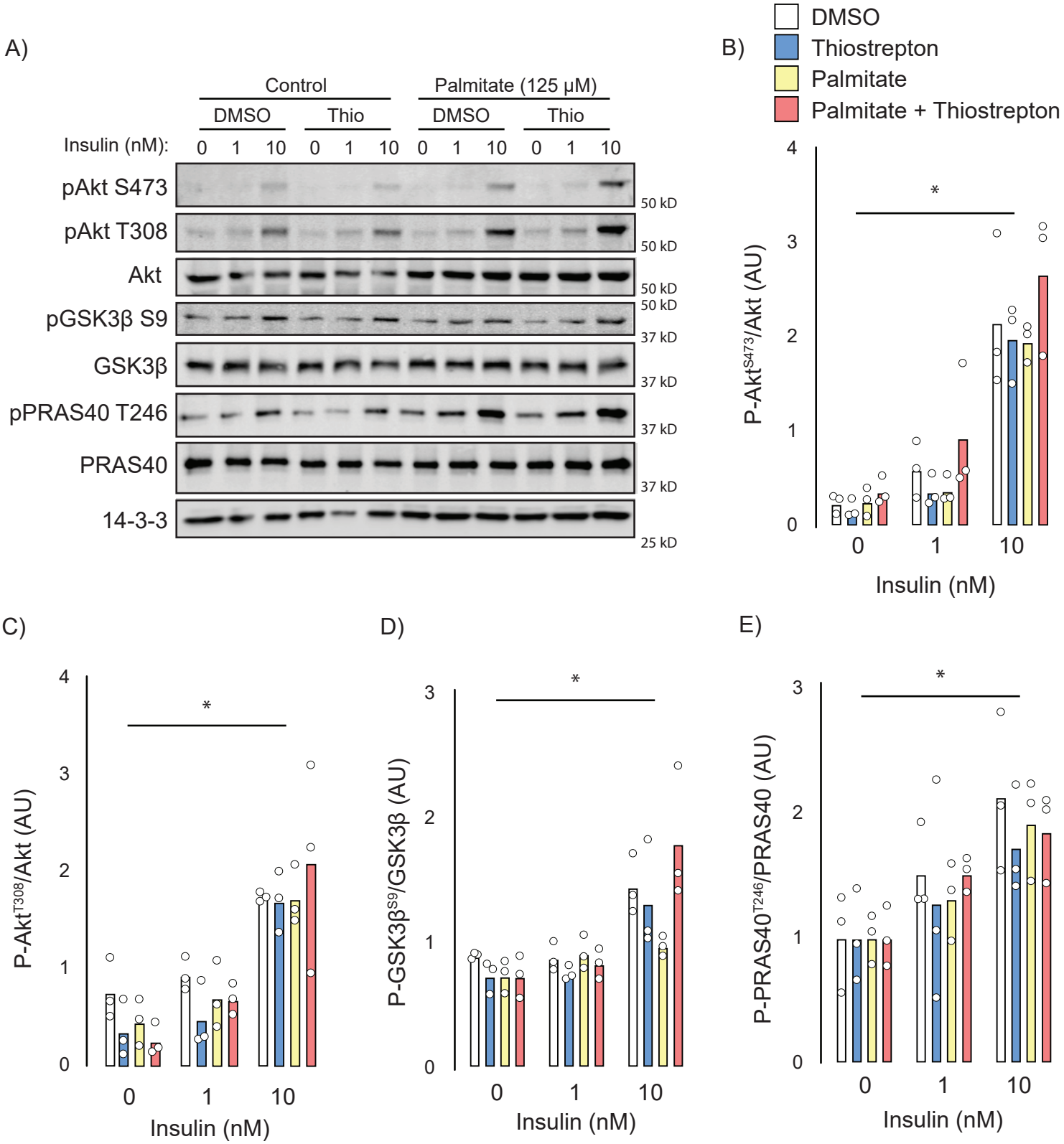

Figure 7

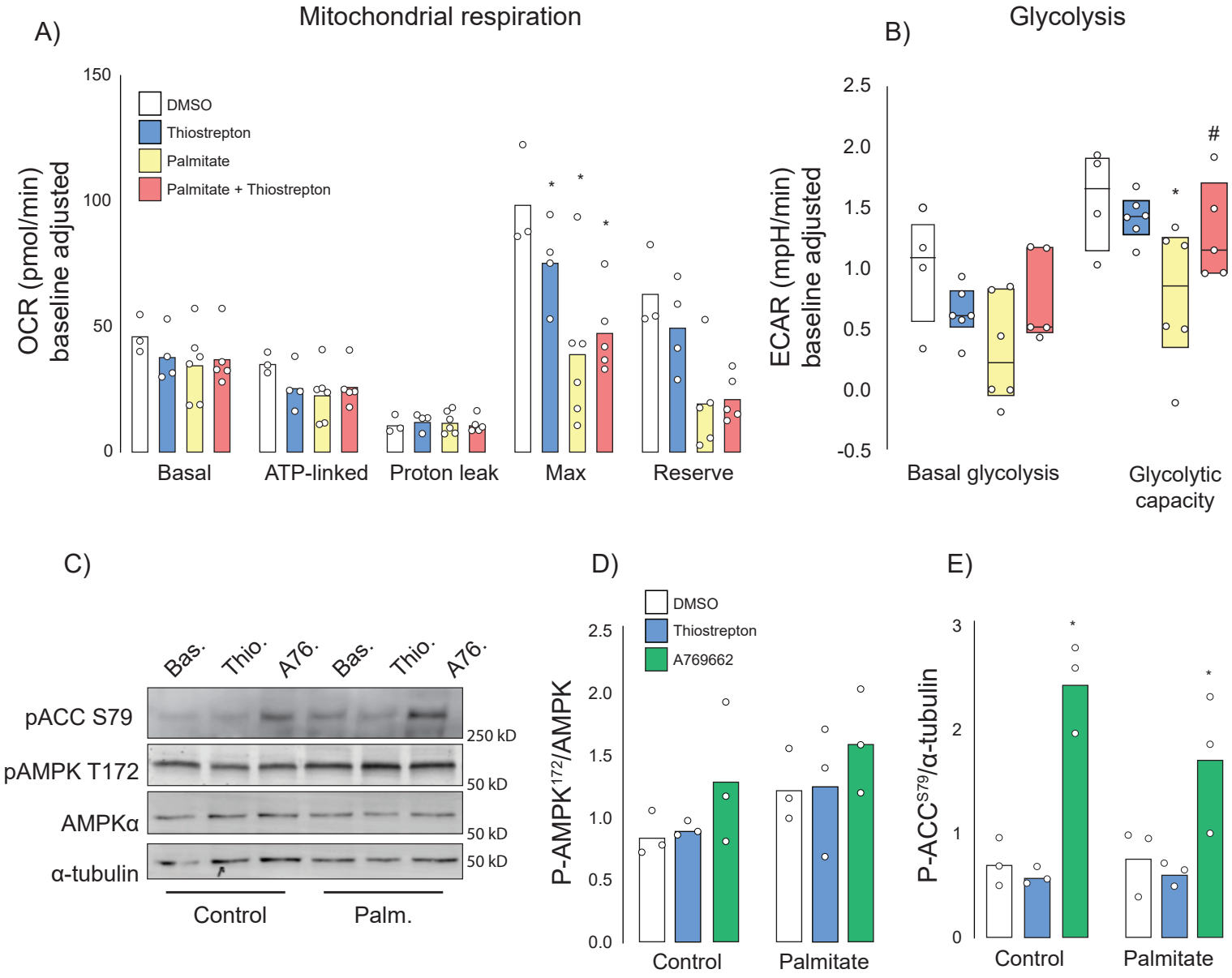

Supplementary Figure 1:

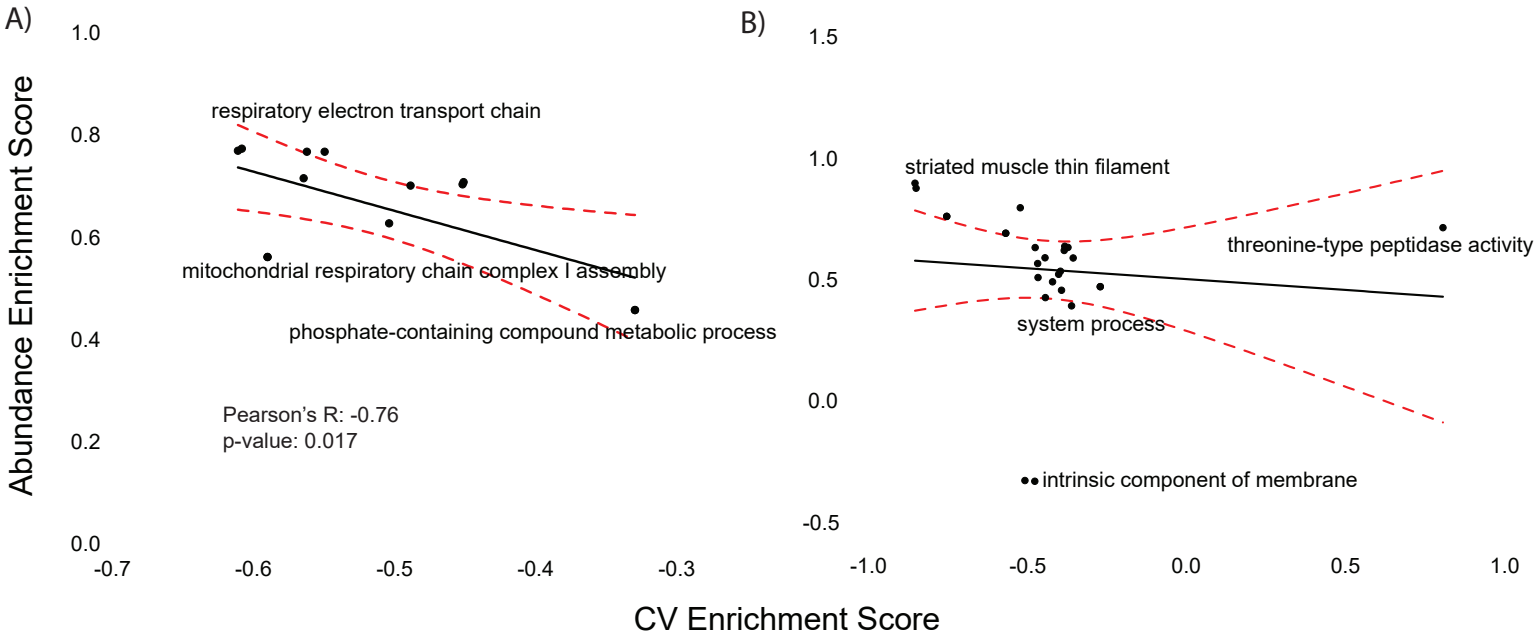

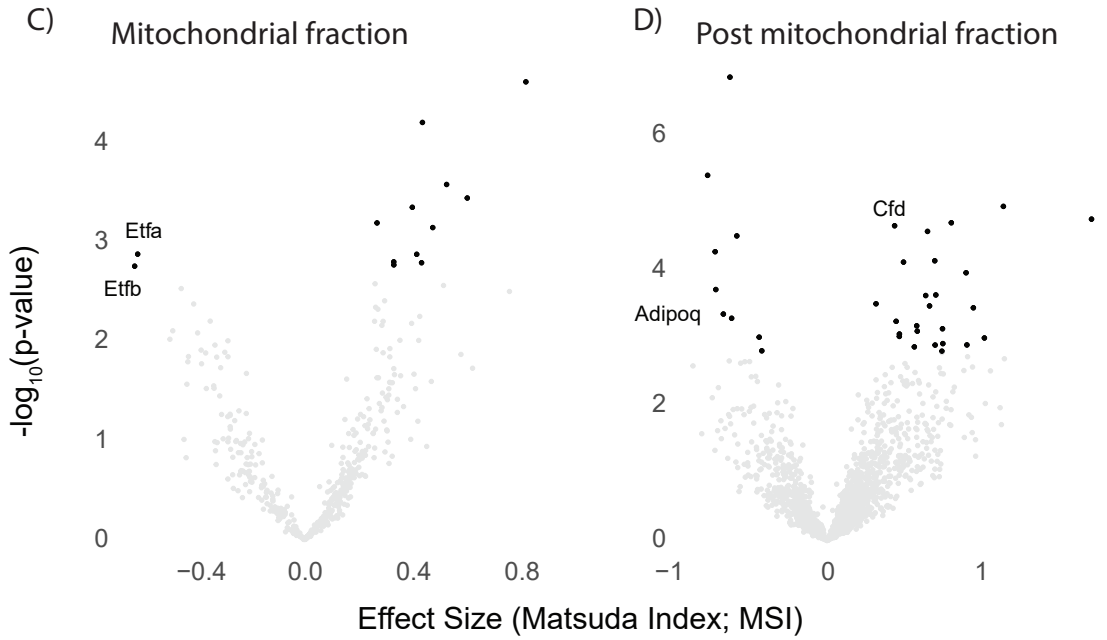

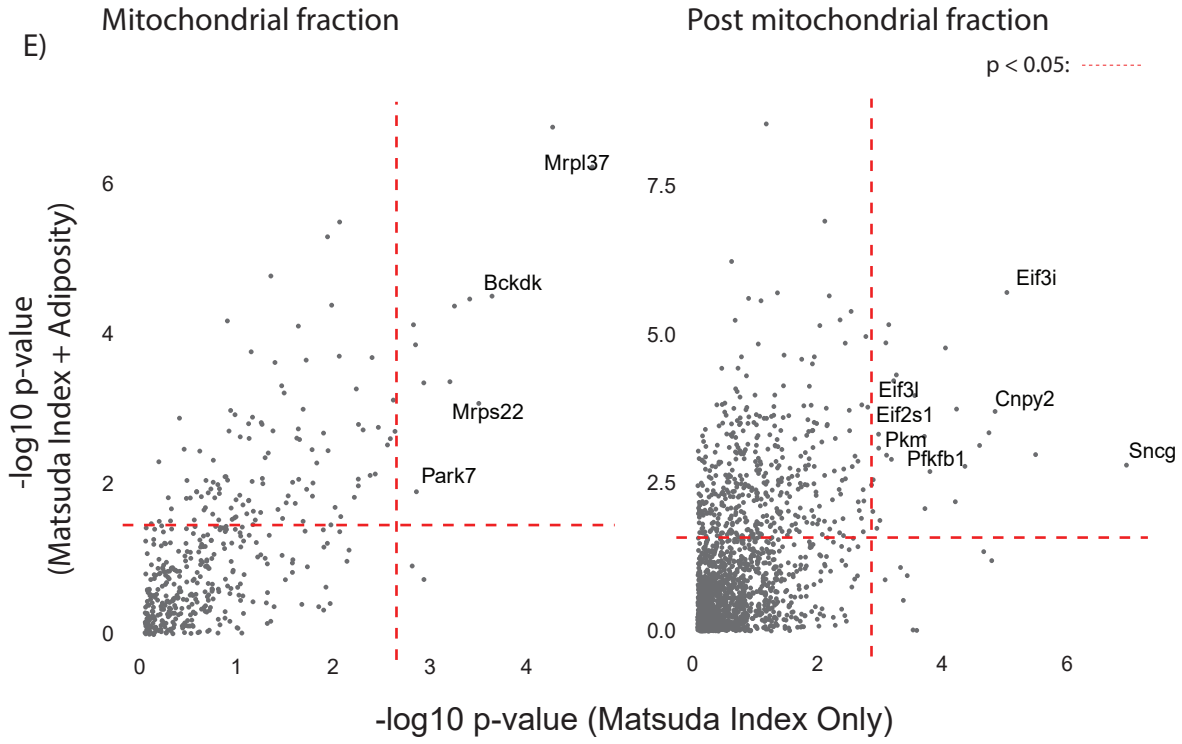

Supplementary Figure 2.

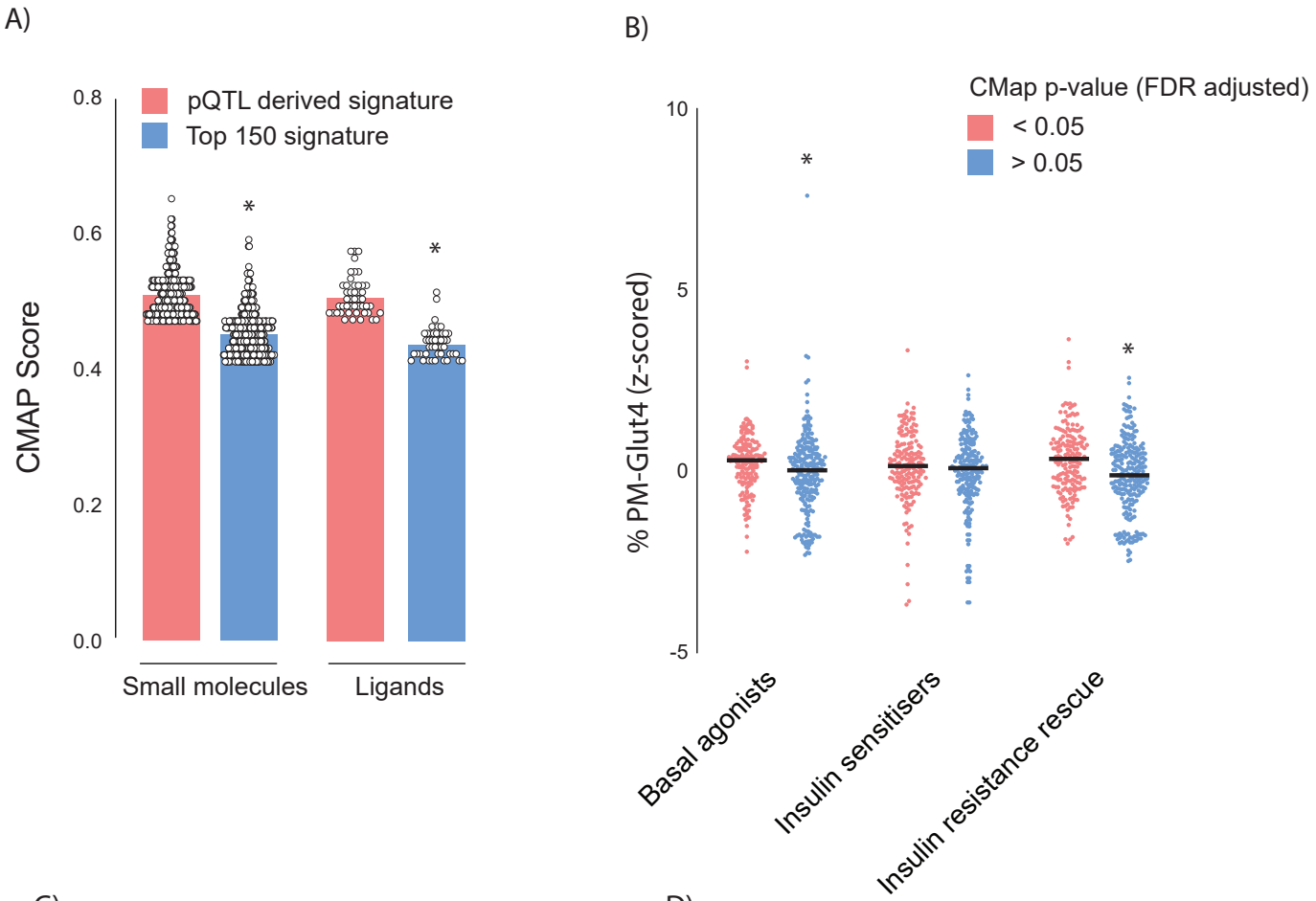

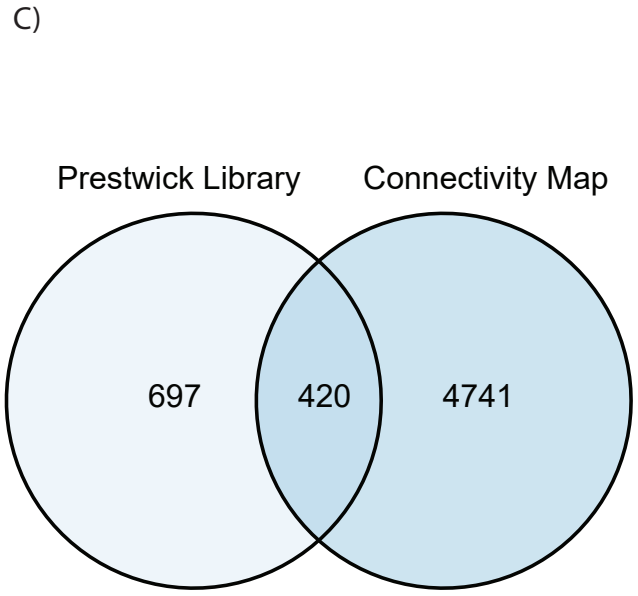

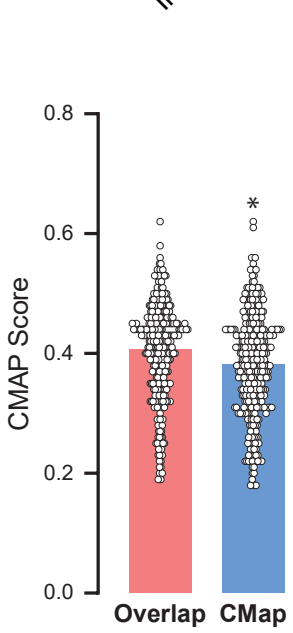

Supplementary Figure 3: